Theory of Electrochemical Kinetics based on Nonequilibrium Thermodynamics

Martin Z. Bazant*

Departments of Chemical Engineering and Mathematics, Massachusetts Institute of Technology, Cambridge, Massachusetts 02139, USA

E-mail: bazant@mit.edu

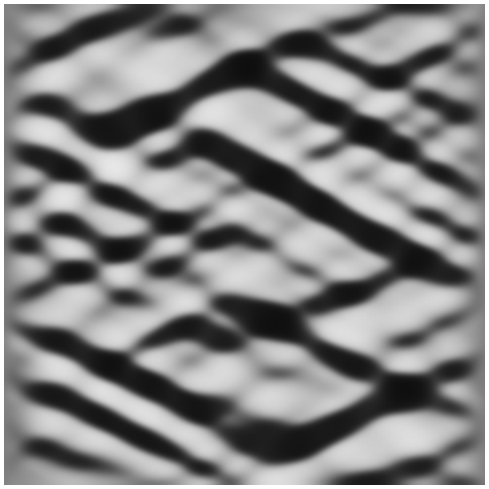

CONSPECTUS

Interest in electrochemistry is surging, driven by new applications in energy conversion, water treatment, materials processing, and biotechnology. As geometries shrink to the nanoscale, the rate-limiting step is often ion intercalation (i.e. reversible insertion) into a host solid for transport or storage. For example, oxygen intercalates into a ceramic electrolytes in solid oxide fuel cells,

*To whom correspondence should be addressed

and lithium intercalates into carbon or metal oxide nanoparticles in Li-ion batteries. The standard phenomenological model for electrode kinetics is the Butler-Volmer equation, which fits the current-voltage relation in many situations and can be justified (in certain limits) by the Marcus theory of charge transfer. Existing theories, however, provide little guidance as to the form of the exchange-current prefactor to account for configurational entropy, elastic stress, phase transformations, and other non-idealities arising in ion intercalation.

These challenges are exemplified by the high-rate cathode material, Li_xFePO_4 (LFP), which has a strong tendency to phase separate into Li-rich and Li-poor phases believed to limit its performance. Phase separation was originally thought to occur as an isotropic “shrinking core" in each particle, but experiments later revealed striped phase boundaries along the active surface. Meanwhile, dramatic rate enhancement was attained with LFP nanoparticles, but no theory could predict the role of phase separation, far from equilibrium. In this Account, a general theory of charge transfer is described, which answers this question and provides a modeling framework for Faradaic reactions in ionic solids and concentrated solutions.

The theory is based on non-equilibrium thermodynamics. The Butler-Volmer and Marcus theories are reformulated in terms of activities and applied to lithium insertion in Li-ion batteries, electrocatalysis in solid oxide fuel cells, and charge transfer in ionic liquids. The Nernst potential and activation overpotential are defined variationally, consistent with Cahn-Hilliard (or Landau-Ginzburg) phase-field models. Unlike classical models, the reaction rate depends on concentration gradients, elastic strain, and surface tension, leading to many surprising conclusions for LFP nanoparticles. At low currents, “intercalation waves" travel across the active surface, but, above a critical current (close to the exchange current), phase separation is suppressed in favor of homogeneous intercalation. Similarly, in porous electrodes, stochastic phase-transformation fronts at low currents are broadened and stabilized at high currents. These complex phenomena can only be described by a unified theory of electrochemical kinetics, thermodynamics and transport.

Introduction

Motivation. Since the seminal work of J. A. V. Butler[1] and M. Volmer,[2] the equation that bears their names,

$$I = I_0 \left(e^{-\alpha_c ne\eta/k_BT} - e^{\alpha_a ne\eta/k_BT} \right) \tag{1}$$

has become the standard phenomenological description of electrode kinetics.[3–5] (Rather than using molar quantities, we define activities per particle and scale potentials to the thermal voltage, $k_BT/e = RT/F$, where k_B = Boltzmann's constant, e = elementary charge, T = temperature.) The Butler-Volmer (BV) equation relates the total current I due to the Faradaic reaction, $O + ne^- \to R$, which converts the oxidized state O to the reduced state R and consumes n electrons, to the exchange current I_0 and overpotential $\eta = \Delta\phi - \Delta\phi^{eq}$, where $\Delta\phi$ is the interfacial voltage whose Nernst equilibrium value is $\Delta\phi^{eq}$. For a simple single-step charge-transfer reaction, the anodic and cathodic charge-transfer coefficients α_a and α_c should satisfy $\alpha_a = 1 - \alpha$ and $\alpha_c = \alpha$ with a symmetry factor, $0 < \alpha < 1$, although the same form is often fitted to more complicated experimental voltage dependence.

The microscopic theory of charge transfer,[6] pioneered R. A. Marcus in 1956[7,8] and honored by the Nobel Prize in Chemistry,[9] provides partial justification for the BV equation and a means to estimate its parameters.[3] The key quantity controlling I_0 and α is the reorganization energy of the solvent upon charge transfer. The theory has been given a quantum mechanical basis by V. G. Levich, R. R. Dogonadze, A. M. Kuznetsov, J. Ulstrup and many others.[6] Marcus theory has been widely applied to dilute solutions, where charge transfer occurs between isolated reactants, but provides little guidance on how to describe correlations in concentrated solutions.

In popular Li-ion battery models,[5,10–13] excluded volume effects are described by an extra concentration factor,

$$I_0(c) = k(c_{max} - c)^{\alpha_c} c^{\alpha_a} \tag{2}$$

where c_{max} is the maximum concentration. The Nernst potential $\Delta\phi^{eq}(c)$ is fitted to the battery open circuit voltage, and the chemical diffusivity $D^{chem}(c)$ of Li in the solid is adjusted to fit

discharge data. In a thermodynamically consistent theory, however, these properties are not independent and should all derive from the lithium activity.

A more systematic approach could be based on non-equilibrium thermodynamics[14,15] and phase-field models.[16] A number of groups have recently made important progress in this direction for electrochemical systems[17–25] and electrokinetic phenomena,[26–34] but without consistently reformulating reaction kinetics. This Account summarizes my struggle to develop such a theory over the past five years,[26,35–43] combining charge-transfer theory[6] with concepts from statistical physics[44,45] and non-equilibrium thermodynamics.[14–16]

Advances in Li-ion batteries increasingly rely on controlling electrochemistry at the nanoscale .[46–49] This trend is well illustrated by lithium iron phosphate, Li_xFePO_4 (LFP), which provided the motivation for my work. In the first LFP paper in 1997, Padhi et al.[50] concluded that "the material is very good for *low-power* applications" but "at higher current densities there is a reversible decrease in capacity that... is associated with the movement of a two-phase interface" (between Li-rich and Li-poor phases). Largely due to shrinking the particle size below 100nm, however, LFP has become the most popular *high-power* cathode material,[51,52] capable of 10 second discharge.[53] Explaining this incredible reversal of fortune turned out to be a major scientific challenge.

We now understand that phase separation is strongly suppressed in LFP nanoparticles, to some extent in equilibrium,[39,41,54] but especially under applied current,[40,41,55,56] since reaction limitation,[37] anisotropic lithium transport,[57,58] elastic coherency strain,[41,43,59,60] and surface energy[40,61,62] are enhanced. At low currents, however, anisotropic nucleation and growth can also occur in nanoparticles,[37,40,41,63] leading to stochastic multi-particle intercalation.[42,64–66] These phenomena could not be described by traditional battery models,[5,10] where the voltage plateau is fitted empirically and the phase boundary is artificially placed, as a spherical "shrinking core".[12,13] In order to develop a predictive model of intercalation in LFP nanoparticles,[41] it was necessary to develop a phase-field theory of electrochemical kinetics,[26,35,40] which is the focus of this Account.

History of this Work. I still remember the day in 2006 when my postdoc, Gogi Singh, brought me the paper of Chen et al.[67] revealing striped phase boundaries in LFP, looking nothing

like a shrinking core. The images suggested phase boundary motion perpendicular to the lithium flux, which, I realized, could not be described by standard chemical kinetics, since the reaction rate would need to depend on concentration *gradients*. Our collaborator, G. Ceder, suggested adapting the CH model for bulk phase separation,[20] but it took several years to achieve a consistent theory. Our initial model predicted intercalation waves,[36–38] but did not uphold the De Donder relation,[44] as became clear from K. Sekimoto and D. Lacoste at ESPCI in Paris. It was there in 2007, while on sabbatical leave, that I first succeeded at generalizing BV kinetics to concentrated solutions. I spent the next year developing dynamical models of concentrated electrochemical systems,[26] not only in batteries and fuel cells, but also induced-charge electrokinetics.[68–70] In spring 2009, I synthesized the theory in lecture notes[35,71] and published the generalized BV equation[26] (Sec. 5.4.2).

The theory has enabled breakthroughs in modeling phase-separating battery electrodes. D. Burch used a thermodynamically consistent “Cahn-Hilliard-Reaction" model to study intercalation in nanoparticles[39] (with $\alpha = 0$), without connections to the battery voltage. His Ph.D. thesis[66] included early simulations of multi-particle phase separation and “mosaic instability" .[64,65] Simulations of galvanostatic discharge by P. Bai and D. A. Cogswell led to a theory of the suppression of phase separation in nanoparticles,[40] first reported in 2010,[72,73] which Cogswell extended for coherency strain.[41] T. R. Ferguson did the first simulations of phase separation and voltage hysteresis in porous electrodes.[42]

This Account provides an overview of the theory and its key predictions. A thermodynamic framework for reaction kinetics and diffusion is applied to Faradaic reactions, and the resulting BV model given microscopic justification via a reformulation of Marcus theory. The theory is then applied to Li-ion batteries, solid-oxide fuel cells, and ionic liquids. Finally, the theory is used to relate electrode kinetics to thermodynamic variational principles and applied to phase-separating battery materials.

Reaction Kinetics in Concentrated Solutions

Nonequilibrium thermodynamics. The theory begins with the diffusional chemical potential of species i,

$$\mu_i = k_B T \ln c_i + \mu_i^{ex} = k_B T \ln a_i \tag{3}$$

where c_i is the concentration, a_i is the absolute chemical activity, $\mu_i^{ex} = k_B T \ln \gamma_i$ is the excess chemical potential in a concentrated solution, and γ_i is the activity coefficient ($a_i = \gamma_i c_i$). In linear irreversible thermodynamics (LIT),[14–16] the flux of species i is proportional to its chemical potential gradient,

$$F_i = -M_i c_i \nabla \mu_i = -D_i \left(\nabla c_i + c_i \nabla \frac{\mu_i^{ex}}{k_B T} \right) = -D_i^{chem} \nabla c_i \tag{4}$$

where D_i is the tracer diffusivity, $M_i = D_i / k_B T$ is the mobility (using the Einstein relation), and $-\nabla \mu_i^{ex}$ is the thermodynamic driving force beyond ideal diffusion (first term). The chemical diffusivity, D^{chem}, differs from the tracer diffusivity by the thermodynamic factor,[5]

$$\frac{D_i^{chem}}{D_i} = 1 + \frac{c_i}{\gamma_i} \frac{\partial \gamma_i}{\partial c_i} = 1 + \frac{\partial \ln \gamma_i}{\partial \ln c_i}. \tag{5}$$

By including the mean electrostatic energy ($z_i e \phi$ below) in the *electro*-chemical potential, this approach has been widely used to describe concentrated solutions in batteries[5,10,13,21–25] and double-layer electrokinetic phenomena.[26–34]

As shown in Eq. (4) and Eq. (5), the total flux has two contributions: (i) free diffusion driven by concentration gradients (Fick's law), and (ii) migration induced by gradients in *excess* chemical potential. In probability theory, the former is the fundamental Wiener process, while the latter is a drift, described by Ito or Stratonovich differentials.[45] In stochastic kinetics,[6,45,74] the reaction complex makes random transitions between local minima in an energy landscape, $U(x)$, which is independent of temperature and neglects many-body interactions. To account for thermal effects, transition state theory for solids[75,76] introduces harmonic contributions to the many-body poten-

tial energy, analogous to “structural relaxation" in Marcus theory[3,9] (discussed below). What is missing in this approach, however, is the effect of configurational entropy or other non-idealities contained in $\mu^{ex}(x)$, which may be obtained from finite-temperature molecular simulations.[76]

In a thermodynamically consistent formulation of reaction kinetics,[35,44] therefore, the reaction complex explores a landscape of *excess* chemical potential $\mu^{ex}(x)$ between local minima μ_1^{ex} and μ_2^{ex} with transitions over an activation barrier $\mu_\ddagger^{ex}$ (Figure 1(a)). Assuming long-lived states with rare transitions ($\mu_\ddagger^{ex} - \mu_i^{ex} \gg k_BT$), the net reaction rate is given by

$$\begin{aligned} R &= R_{1\to 2} - R_{2\to 1} \\ &= \nu\left[c_1 e^{-(\mu_\ddagger^{ex}-\mu_1^{ex})/k_BT} - c_2 e^{-(\mu_\ddagger^{ex}-\mu_2^{ex})/k_BT}\right] \\ &= \nu\left[e^{-(\mu_\ddagger^{ex}-\mu_1)/k_BT} - e^{-(\mu_\ddagger^{ex}-\mu_2)/k_BT}\right] \\ &= \frac{\nu(a_1-a_2)}{\gamma_\ddagger} \end{aligned} \tag{6}$$

which automatically satisfies the De Donder relation,[44] $\mu_1 - \mu_2 = k_BT\ln(R_{1\to 2}/R_{2\to 1})$. The frequency prefactor ν depends on generalized force constants, $k_i = \frac{\partial^2 \mu^{ex}}{\partial x_i^2}$, or effective lengths $\ell_i = \sqrt{\frac{2\pi k_BT}{k_i}}$, at the saddle point and in one minimum (e.g. state 1, with a suitable shift of $\mu_\ddagger^{ex}$). Extending Kramers' escape formula[45,77] to N reaction coordinates $x_1,...,x_N$, we find

$$\nu = \frac{k^{\|}\prod_{i=1}^{N} k_i^{min}}{2\pi\zeta_f \prod_{j=1}^{N-1} k_j^{\perp}} = \frac{D_f \prod_{i=1}^{N-1} L_i^{\perp}}{L^{\|}\prod_{i=1}^{N} L_i^{min}} \tag{7}$$

where k_i^{min} are curvatures at the minimum (normal modes), $k_j^{\perp}$ are positive, transverse saddle curvatures, and $-k^{\|}$ is the negative saddle curvature parallel to the transition path. The rate increases with k_i^{min} (due to faster vibrations and thus more frequent escape attempts) and $k^{\perp}$ (due to less time spent near the saddle), and decreases with $k_j^{\perp}$ (due to fewer trajectories captured with k_BT of the saddle). The effect of $k^{\perp}$ from stochastic kinetics[45] is missing in classical transition state theory,[75,76] but it is often negligible in charge-transfer reactions,[6,78] due to the Franck-Condon principle that electron transfer occurs suddenly when vibrational states overlap (or at an even lower

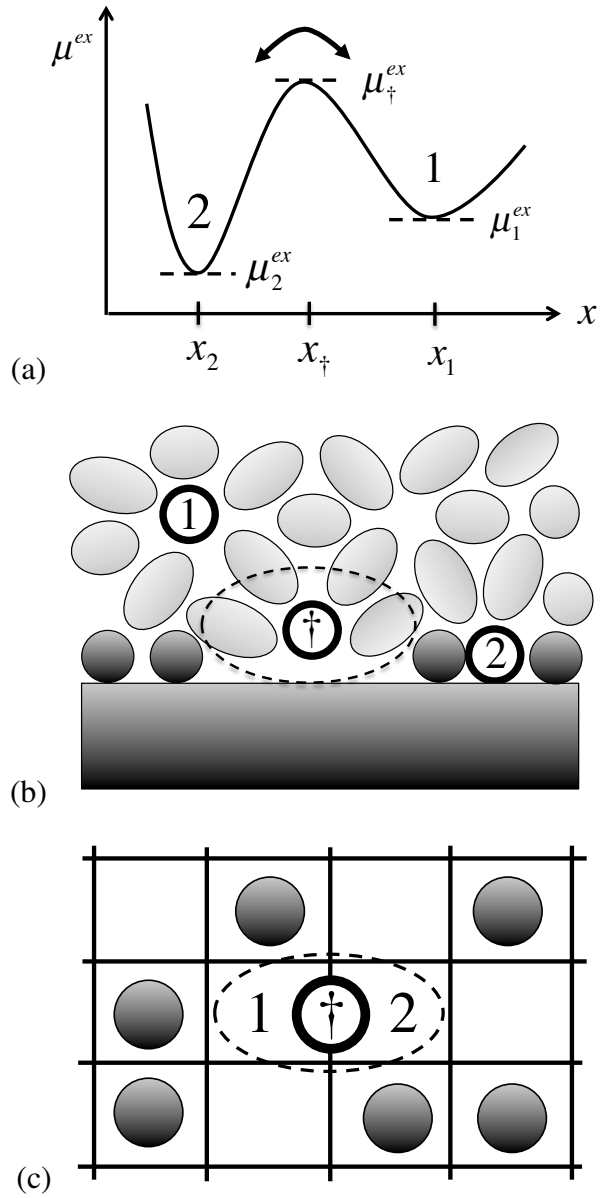

Figure 1: Reaction kinetics in concentrated solutions. (a) The reaction complex moves in a landscape of *excess* chemical potential from state 1 to state 2 over a barrier (transition state). (b) Surface adsorption (or intercalation in a solid solution) from a liquid, where the transition state excludes $s > 1$ particle volumes as in Eq. (13), e.g. to accommodate the shedding of the solvation shell. (c) Activated diffusion on a surface (or in a solid solution), where the transition state excludes two particle sites and thus Eq. (15) reduces to Eq. (16).

energy, below the saddle point, due to quantum tunneling). This concept is the basis for Marcus theory below. In a liquid, the friction coefficient can be estimated by the Stokes-Einstein relation, $\zeta_f = \frac{k_B T}{D_f} \approx 6\pi\eta a$, where η is the shear viscosity and a is the molecular size.[74]

For the general reaction,

$$S_1 = \sum_i s_i M_i \rightarrow \sum_j s_j M_j = S_2, \tag{8}$$

the activities,

$$a_1 = \prod_i a_i^{s_i} \quad \text{and} \quad a_2 = \prod_j a_j^{s_j}, \tag{9}$$

are equal in equilibrium, and the forward and backward reactions are in detailed balance ($R = 0$). The equilibrium constant is thus the ratio of the reactant to product activity coefficients:

$$K = \frac{c_2}{c_1} = \frac{\prod_j c_j^{s_j}}{\prod_i c_i^{s_i}} = \frac{\prod_i \gamma_i^{s_i}}{\prod_j \gamma_j^{s_j}} = \frac{\gamma_1}{\gamma_2} = e^{(\mu_1^{ex} - \mu_2^{ex})/k_B T} = e^{-\Delta G^{ex}/k_B T} \tag{10}$$

where ΔG^{ex} is the *excess* free energy change per reaction. In order to describe reaction kinetics, however, we also need a model for the transition state activity coefficient $\gamma_\ddagger$, in Figure 1).

The subtle difference between total and excess chemical potential is often overlooked in chemical kinetics. Lai and Ciucci,[23–25] who also recently applied non-equilibrium thermodynamics to batteries, start with the same flux relation, Eq. (4), but postulate a Faradaic reaction rate based on a barrier of total (not excess) chemical potential. The equilibrium condition (Nernst equation) is the same, but the rate (exchange current) is different and does not consistently treat the transition state. These concepts become more clear for adsorption phenomena without charge transfer, as we now illustrate.

Surface or solid intercalation. Consider surface adsorption from a liquid, or, equivalently, intercalation in the surface layer of a solid solution (Figure 1(b)). The standard approach in chemistry is to write the reaction as $M + V_s \rightarrow M_s$, where V_s is a vacant surface site, and assume first-order kinetics,

$$R = k\left[K c_M (1-c) - c\right], \tag{11}$$

where c is now the surface coverage (or solid filling fraction), $K = e^{E_a/k_BT}$ is the equilibrium constant and E_a the adsorption energy. In detailed balance, $R = 0$, this implies a Langmuir isotherm, $c^{eq} = Kc_M/(1+Kc_M)$.

In our approach, rather than assigning a chemical identity to the vacancy, we consider the reaction $M \to M_s$. In order to recover the Langmuir isotherm from the equilibrium condition, $\mu_1 = \mu_2$, we write diffusional chemical potentials for species M in the liquid, $\mu_1 = k_BT \ln(Kc_M)$ (as a dilute solution), and on the surface,

$$\mu_2 = k_BT \ln \frac{c}{1-c}, \quad \text{or} \quad \gamma = \frac{1}{1-c} \tag{12}$$

as a lattice gas, or ideal solid solution.[16] We then consistently model $\mu_\ddagger^{ex}$. For example, if the transition state has energy $E_\ddagger$ relative to the adsorbed state and excludes a volume $s \geq 1$ surface sites (not necessarily an integer), e.g. while shedding a solvation shell, then

$$\mu_\ddagger^{ex} = E_\ddagger - sk_BT \ln(1-c), \quad \text{or} \quad \gamma_\ddagger = \frac{e^{E_\ddagger/k_BT}}{(1-c)^s}. \tag{13}$$

Plugging into Figure 1, we obtain the reaction rate,

$$R = k\left[Kc_M(1-c)^s - c(1-c)^{s-1}\right], \quad \text{where} \quad k = \nu e^{-E_\ddagger/k_BT}, \tag{14}$$

which differs from Eq. (11) if $s \neq 1$. In this simple case, for integer s, a similar form follows from Flory-Huggins kinetics[4] with a higher-order vacancy reaction, $M + sV_s \to M_s + (s-1)V_s$, but the general theory is needed for more complicated situations. For example, if adsorption occurs between disordered liquid and solid states, then the excluded volume cannot be treated as a distinct chemical species, but one could still use hard-sphere models for the excess chemical potentials in the present theory, as illustrated below.

Surface or solid diffusion. On a surface or in a solid solution, diffusion occurs by thermally activated hopping between adjacent sites[76] (Figure 1(c)). The flux $F_i = -R/A_s$ through a cell

area A_s follows from Figure 1 by linearizing $a_2 - a_1 \approx \Delta x \frac{\partial a}{\partial x}$. Comparing with Eq. (4), the tracer diffusivity is given by

$$D_i = \frac{\nu \Delta x^2 \gamma}{\gamma_{\ddagger}}, \tag{15}$$

In an ideal solid solution (Eq. (12)), the transition state excludes two sites ($s = 2$ in Eq. (13)) before and after the hop. The tracer diffusivity Eq. (15) then scales with the density of vacancies,

$$D_i = D_i^0 (1 - c), \quad \text{where} \quad D_i^0 = \nu \Delta x^2 e^{\Delta E_{\ddagger}/k_B T} \tag{16}$$

is the tracer diffusivity in a dilute solution. Due to a remarkable cancellation, the chemical diffusivity (Eq. (5)) is constant,

$$D_i^{chem} = \frac{D_i}{1 - c} = D_i^0 \tag{17}$$

and equal to the dilute-limit tracer diffusivity of particles or vacancies. Nauman[79] made thermodynamic arguments to show that the $(1 - c)$ factor in Eq. (16) should appear in the Cahn-Hilliard equation (discussed below), and here we see it follow from our reaction model Figure 1. This factor should also appear in the modified Poisson-Nernst-Planck equations for a solid solution.[31]

Butler-Volmer Kinetics in Concentrated Solutions

For the general electrode reaction,

$$S_1 = O^{z_O} + ne^- \rightarrow R^{z_R} = S_2 \tag{18}$$

we write $\mu_1 = \mu_O + n\mu_e$ and $\mu_2 = \mu_R$, where charge conservation implies $z_O - n = z_R$. We decompose the *electro*-chemical potential into chemical and electrostatic contributions,

$$\mu_i = k_B T \ln a_i + z_i e \phi_i = (k_B T \ln c_i + z_i e \phi_i) + \mu_i^{ex} \tag{19}$$

where the term in parentheses describes an ion of charge $z_i e$ in a mean potential ϕ_i in a dilute solution, and $\mu_i^{ex} = k_B T \ln \gamma_i$ is the excess chemical potential. The electrostatic potential of the electrode is ϕ_e, while that of the electrolytic solution is ϕ. The difference is the interfacial voltage, $\Delta\phi = \phi_e - \phi$.

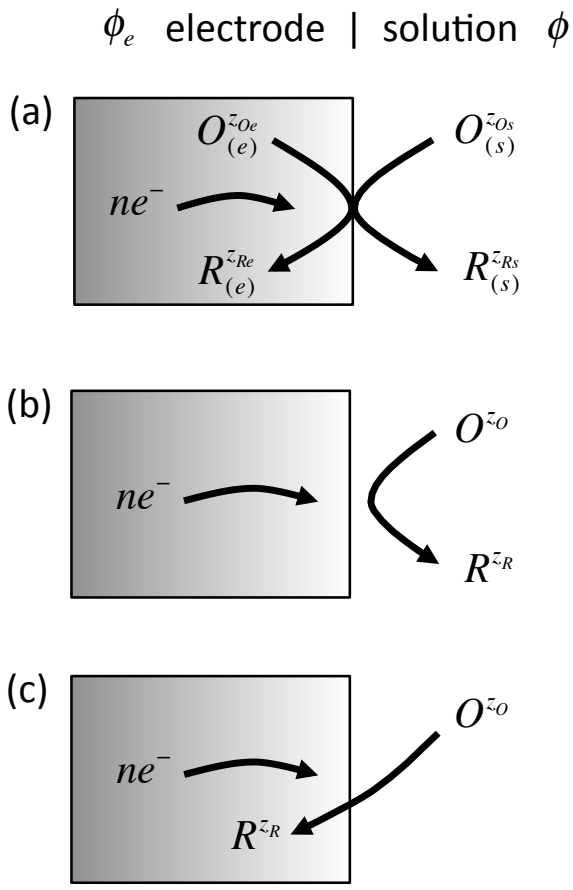

Figure 2: Types of Faradaic reactions. (a) The most general reaction involving reduced and oxidized molecules, each split between the electrode and the electron-free electrolytic solution. (b) Redox reaction in solution. (c) Insertion or electrodeposition, where the reduced state lies inside or on the surface of the electrode, respectively.

The electric field $E = -\nabla\phi$ at point is unique, so the potential ϕ_i of species i depends its position with respect to the interface. By definition, the electrons come from the electrode with potential ϕ_e, but ions can exist in either position. In the most general Faradaic reaction (Figure 2(a)), the reduced and oxidized states can be split between the electrode and solution phases, $O^{z_O} = O^{z_{Oe}}_{(e)} + O^{z_{Os}}_{(s)}$ and $R^{z_R} = R^{z_{Re}}_{(e)} + R^{z_{Rs}}_{(s)}$, if the electrode is a mixed ion-electron conductor. The

solution species, $O_{(s)}^{z_{Os}}$ and $R_{(s)}^{z_{Rs}}$, are at potential ϕ and electrode species, $O_{(e)}^{z_{Oe}}$ and $R_{(e)}^{z_{Re}}$, are at potential ϕ_e. Charge conservation implies $z_{Oe} + z_{Os} - n = z_{Re} + z_{Rs}$. The net charge $n_c e$ transferred from the solution to the electrode is given by

$$n_c = z_{Os} - z_{Rs} = z_{Re} - z_{Oe} + n. \tag{20}$$

In this Account, we focus on situations where the oxidized state exists only in the solution ($z_{Oe} = 0$). In the simplest case of a redox reaction in solution (Figure 2(b)), there are no ions in the electrode and thus $n_c = n$. In electrodeposition, the reduced state is a neutral species on the surface ($z_R = 0$), so $n_c = n = z_O$. For cation insertion (Fig. Figure 2(c)), the reduced state is an intercalated ion, and the charge transferred across the interface is $n_c = z_O$.

In many cases, the interfacial charge transfer is equal to the number of electrons, $n_c = n$, and we can set $\phi_R = \phi_O = \phi$ without loss of generality, due to neutral reactants or products. Besides electrodeposition, we shall consider lithium ion insertion in a neutral crystal ($n_c = n = 1$, $z_R = 0$) and oxygen reduction in a solid electrolyte ($n_c = n = -z_R = 2$, $z_O = 0$). For this broad class of Faradaic reactions, the electrochemical potentials of the species in Eq. (18) are

$$\mu_O = k_B T \ln a_O + z_O e \phi \tag{21}$$

$$\mu_R = k_B T \ln a_R + z_R e \phi \tag{22}$$

$$\mu_e = k_B T \ln a_e - e \phi_e \tag{23}$$

where μ_e is the chemical potential of electrons, or Fermi level. The electron activity $a_e = \gamma_e c_e$ accounts for the concentration of free electrons c_e (density of states), as well as shifts in the Fermi level via γ_e, due to applied stress, phase transformations, donor or acceptor ions, etc. as illustrated below for semiconducting electrodes.

In equilibrium ($\mu_1 = \mu_2$), the interfacial voltage, $\Delta\phi = \phi_e - \phi$, satisfies the Nernst equation

$$\Delta\phi^{eq} = \frac{k_B T}{n_c e} \ln \frac{a_O a_e^n}{a_R} \tag{24}$$

where $n_c = n$. Out of equilibrium, the current $I = neAR$ (where $A =$ electrode area) is related to the local (activation, or surface) over-potential,

$$\eta = \Delta\phi - \Delta\phi^{eq} \tag{25}$$

Specific models of charge transfer correspond to different choices of $\mu_{\ddagger}^{ex}$.

In order to generalize Butler-Volmer kinetics, we approximate the mean electrostatic energy of the transition state as a linear combination of those of the initial and final states:

$$\mu_{\ddagger}^{ex} = k_B T \ln \gamma_{\ddagger} + \alpha_a (z_O e\phi - ne\phi_e) + \alpha_c z_R e\phi \tag{26}$$

If, for consistency, the electric field is constant across the reaction coordinate x from x_R to x_O past the transition state at $x_R < x_{\ddagger} < x_O$, then the transfer coefficients, $\alpha_a = 1 - \alpha$ and $\alpha_c = \alpha$, are related to the symmetry factor,[4]

$$\alpha = \frac{x_{\ddagger} - x_R}{x_O - x_R} = \alpha_c = 1 - \alpha_a, \tag{27}$$

which acts as a Brønsted coefficient.[6]

Substituting Eq. (24)-Eq. (27) into Figure 1, we obtain the BV equation Eq. (1) with

$$I_0 = \frac{\nu neA(a_O a_e^n)^{1-\alpha} a_R^{\alpha}}{\gamma_{\ddagger}} = \left[\nu neA(c_O c_e^n)^{1-\alpha} c_R^{\alpha}\right] \left[\frac{(\gamma_O \gamma_e^n)^{1-\alpha} \gamma_R^{\alpha}}{\gamma^{\ddagger}}\right] \tag{28}$$

The first factor is the classical formula,[3–5] but this is only valid for dilute solutions ($\gamma_O = \gamma_R = \gamma_{\ddagger} = \gamma_e = 1$). The second factor modifies the exchange current for concentrated solutions. In summary, the Faradaic current I is related to the interfacial voltage $\Delta\phi$ and the various chemical activities a_O, a_R, a_e, and $\gamma_{\ddagger}$ by Eq. (1), Eq. (24), Eq. (25), and Eq. (28).

Marcus Theory for Concentrated Solutions

Just as we have reformulated the phenomenological Butler-Volmer model for concentrated solutions, so it is also possible to adapt the microscopic theory of charge transfer. The basic idea (Figure 3) is that the Faradaic reaction Eq. (18) occurs when the *excess* chemical potential of the reduced state, deformed along the reaction coordinate by statistical fluctuations, equals that of the oxidized state (plus n electrons in the electrode) at the same point. More precisely, charge transfer occurs randomly at somewhat lower energies due to quantum tunneling.[3,6]

As a first approximation,[3,6] we postulate harmonic restoring potentials for structural relaxation (e.g. shedding of the solvation shell from a liquid, or extraction from a solid) along the reaction coordinate x from the oxidized state at x_O to the reduced state at x_R:

$$\mu_1^{ex}(x) = k_B T \ln(\gamma_O \gamma_e^n) + z_O e\phi - ne\phi_e + \frac{k_O}{2}(x - x_O)^2 \tag{29}$$

$$\mu_2^{ex}(x) = k_B T \ln \gamma_R + z_R e\phi + \frac{k_R}{2}(x - x_R)^2 \tag{30}$$

The Nernst equation Eq. (24) follows by equating the chemical potentials at the local minima, $\mu_1(x_O) = k_B T \ln(c_O c_e^n) + \mu_1^{ex}(x_O) = k_B T \ln c_R + \mu_2^{ex}(x_R) = \mu_2(x_R)$ in equilibrium. The free energy barrier is set by the intersection of the excess chemical potential curves for the initial and final states,

$$\mu_\ddagger^{ex} = \mu_1^{ex}(x_\ddagger) = \mu_2^{ex}(x_\ddagger), \tag{31}$$

which is an implicit equation for the barrier position, $x = x_\ddagger$. Combining Eq. (25), Eq. (24), and Eq. (31) we obtain

$$ne\eta - k_B T \ln \frac{c_R}{c_O c_e^n} = \frac{k_O}{2}(x_\ddagger - x_O)^2 - \frac{k_R}{2}(x_\ddagger - x_R)^2 = \mu_2^{ex}(x_R) - \mu_1^{ex}(x_O) = \Delta G^{ex} \tag{32}$$

where ΔG^{ex} is the *excess* free energy change per reaction. The overpotential is the *total* free energy

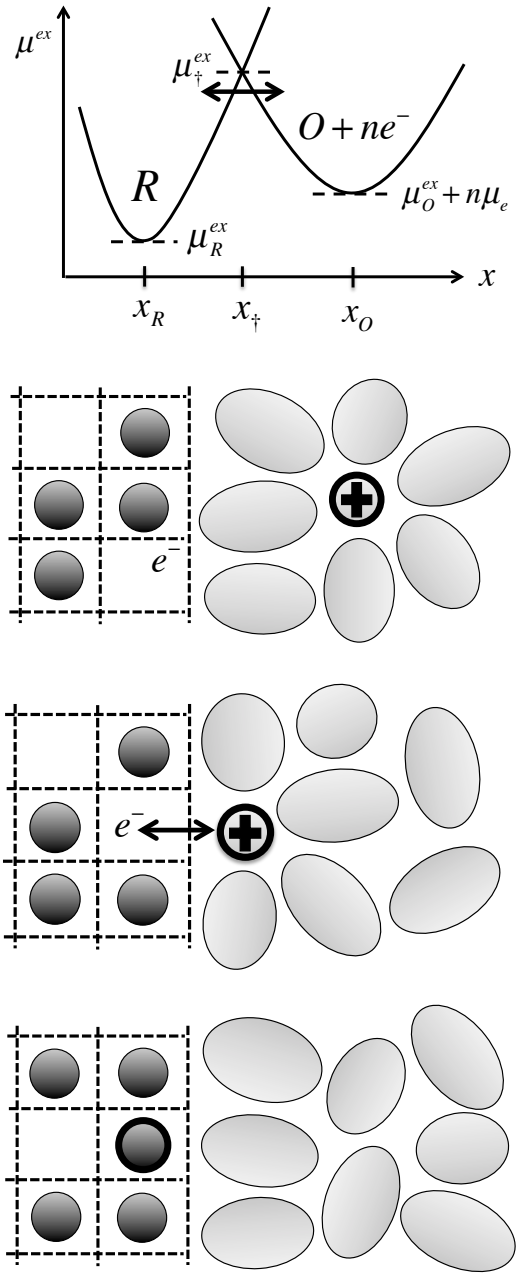

Figure 3: Above: The Faradaic reaction $O + ne^- \rightarrow R$ in concentrated electrolyte and/or electrode solutions. The reactants fluctuate in a landscape of excess chemical potential μ^{ex}, shown along a favored reaction coordinate x. Charge transfer occurs whenever the oxidized state O with n free elections or the reduced state R reaches the transition state. Below: Illustration of these states for ion reduction by intercalation into a solid-solution electrode from a liquid electrolyte.

change per charge transferred,

$$ne\eta = ne\Delta\phi - k_B T \ln \frac{a_O a_e^n}{a_R} = \mu_2(x_O) - \mu_1(x_R) \equiv \Delta G \tag{33}$$

where

$$\Delta G = ne\eta = \Delta G^{ex} + k_B T \ln \frac{c_R}{c_O c_e^n} \tag{34}$$

is the thermodynamic driving force for the reaction. Note that in classical Marcus theory,[3,9] the overpotential is defined by $ne\eta = \Delta G^{ex}$ without the concentration factors required by non-equilibrium thermodynamics. This is correct for charge-transfer reactions in bulk phases, e.g. $A^- + B \rightarrow A + B^-$, because the initial and final concentrations are the same, and thus $\Delta G = \Delta G^{ex} = \Delta G^0$ (standard free energy of reaction). For Faradaic reactions at interfaces, however, the concentrations of reactions and products are different, and Eq. (34) must be used. The missing "Nernst concentration term" in Eq. (34) is also noted by Kuznetsov and Ulstrup (p. 219) in their quantum-mechanical theory of electrochemical kinetics.[6]

Following Marcus, we solve Eq. (32) for $x_\ddagger$ and substitute into Eq. (31) in order to relate $\mu_\ddagger^{ex}$ to η. In the simplest case of symmetric relaxation, $k_O = k_R = k$, we find,

$$\mu_\ddagger^{ex} = k_B T \ln(\gamma_O \gamma_e^n) + z_O e\phi - ne\phi_e + \frac{\lambda}{4}\left(1 + \frac{\Delta G^{ex}}{\lambda}\right)^2 \tag{35}$$

$$= k_B T \ln \gamma_R + z_R e\phi + \frac{\lambda}{4}\left(1 - \frac{\Delta G^{ex}}{\lambda}\right)^2 \tag{36}$$

where

$$\lambda = \frac{k}{2}(x_O - x_R)^2 \tag{37}$$

is the "reorganization energy". The barriers for the cathodic and anodic reactions are,

$$\Delta G_c^{ex} = \frac{\lambda}{4}\left(1 + \frac{\Delta G^{ex}}{\lambda}\right)^2 \tag{38}$$

$$\Delta G_a^{ex} = \frac{\lambda}{4}\left(1 - \frac{\Delta G^{ex}}{\lambda}\right)^2 \tag{39}$$

respectively. Substituting $\mu_{\ddagger}^{ex}$ into Figure 1, the current $I = neAR$ is given by

$$I = I_0 e^{(ne\eta)^2/4k_BT\lambda}\left(e^{-\alpha ne\eta/k_BT} - e^{(1-\alpha)ne\eta/k_BT}\right) \tag{40}$$

which has a stronger nonlinear dependence on overpotential than in the Butler-Volmer equation. The exchange current,

$$I_0 = neAe^{-\lambda/4k_BT}(c_O c_e^n)^{1-\alpha} c_R^{\alpha}, \tag{41}$$

and symmetry factor,

$$\alpha = \frac{1}{2}\left(1 - \frac{k_BT}{\lambda}\right) \tag{42}$$

are both related to the reorganization energy λ. In the typical case, $\lambda \gg k_BT$ (for thermally stable solvation), the symmetric factor is $\alpha \approx \frac{1}{2}$, and the current Eq. (40) is well approximated by the Butler-Volmer equation up to fairly large overpotentials, $|\eta| \ll \frac{k_BT}{ne}\sqrt{\frac{\lambda}{k_BT}}$. Comparing Eq. (41) with Eq. (28), we can relate the reorganization energy to the activity coefficients defined above,

$$\frac{\lambda}{4} = k_BT \ln \frac{\gamma_{\ddagger}}{(\gamma_O \gamma_e^n)^{1-\alpha}\gamma_R^{\alpha}} = (1-\alpha)\Delta G_c^{ex} + \alpha \Delta G_a^{ex} \tag{43}$$

which is an average barrier for the cathodic and anodic reactions, weighted by the symmetry factor.

In a dilute solution, the reorganization energy λ_0 can be estimated by the classical Marcus approximation, $\lambda_0 = \lambda_i + \lambda_o$, where

$$\lambda_i = \sum_m \frac{k_m}{2}(q_{O,m} - q_{R,m})^2 \tag{44}$$

is the “inner" or short-range contribution from structural relaxation (sum over normal modes) and λ_o is the “outer", long-range contribution from dielectric relaxation of the solvent.[3,9] In the Born approximation, the latter is given by

$$\lambda_o = \frac{(ne)^2}{8\pi}\left(\frac{1}{a} - \frac{1}{R}\right)\left(\frac{1}{\varepsilon_{op}} - \frac{1}{\varepsilon_s}\right) \tag{45}$$

for a Faradaic reaction at a flat metal electrode, where ε_s is the (static) permittivity of the bulk solvent, a is the radius of the solvation shell with (optical) permittivity ε_{op}, and R is twice the separation of the ion from the electrode (charge-image distance). Since $\lambda_o = (0.5-1.0)n^2$ eV $\gg k_BT$ for polar solvents at room temperature, the large barrier Eq. (34) implies that single-electron ($n=1$), symmetric ($\alpha \approx \frac{1}{2}$) charge transfer is favored. Many quantum mechanical expressions for λ_0 are also available.[6]

In a concentrated solution, we can use various models below to estimate the thermodynamic correction, $\gamma_\ddagger^c$, due to entropic and enthalpic effects in the transition state. The exchange current can then be modeled by Eq. (28) with

$$\gamma_\ddagger = \gamma_\ddagger^c e^{\lambda_0/4k_BT}. \tag{46}$$

where α given by Eq. (42) with $\lambda = \lambda_0$. For example in surface adsorption, if the transition state excludes s sites, $\gamma_\ddagger^c = (1-c)^{-s}$, then Eq. (46) reduces to Eq. (13) with $E_\ddagger = \frac{\lambda_0}{4}$, consistent with Eq. (43). This approach provides a thermodynamically consistent way to model the combined effects of solvation, structural relaxation, enthalpy and entropy on charge transfer kinetics in a concentrated solution, ionic liquid or solid.

The compositional effects predicted by the general theory are crucial for deposition or intercalation reactions (Figure 4). Dilute solution approximations are widely used to model electrodeposition[80] (Figure 4(a)), but our formulation of electrode kinetics enables the use of phase-field models (below), which are convenient for simulating electrodeposition[17,18,81–83] with dendritic growth.[84–87] With fixed interfaces, the general theory is also required for a thermodynamically consistent treatment of ion intercalation in solid solutions.[39–41]

Ion Intercalation in Solid Solutions

Lithium insertion. The canonical example is reversible lithium insertion, $Li^+ + e^- \rightarrow Li_{(s)}$, in a solid host[35,49] (Figure 4(b)). Although lithium ions often remain charged after insertion, they

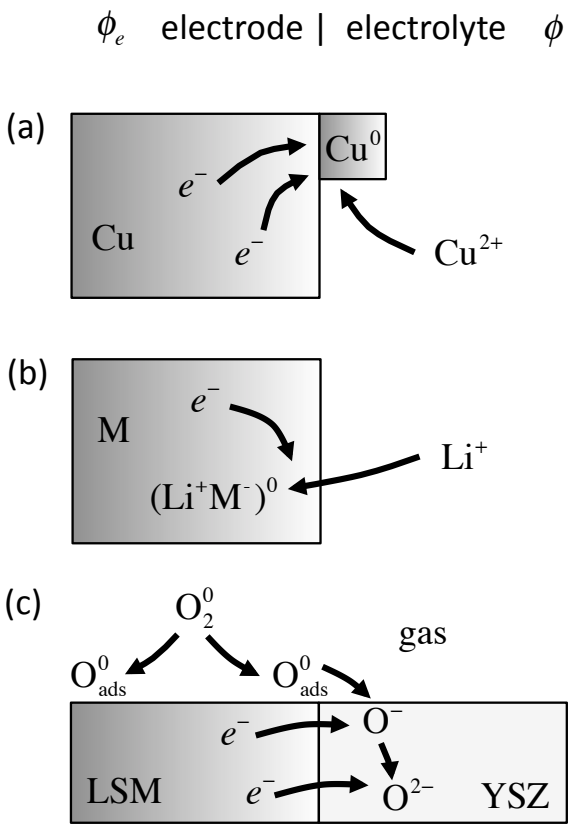

Figure 4: Examples of Faradaic reactions with non-ionic electrodes, $n_c = n$: (a) copper electrodeposition, (b) lithium ion insertion in a transition metal oxide M in a Li-ion battery, (c) oxygen reduction in a solid oxide fuel cell by gas adsorption on the electrode catalyst (LSM), followed by charge transfer and ion intercalation in the solid electrolyte (YSZ).

exist in neutral quasiparticle (polaron[6]) states, Li^+M^-, coupled to reduced M groups in the crystal. Lithium thus acts as a donor impurity, and in some cases, can cause metal-semiconductor transitions (see below). In transition metal oxides, the compensating electron usually resides on a metal ion, e.g. $Fe^{3+} \to Fe^{2+}$ in Li_xFePO_4, or on various dopants or surface coatings. In mixed ion-electron conductors, the separation of Li^+ and M^- leads to diffuse charge near the interface and Frumkin corrections to the reaction rate,[88,89] but we will focus on cases where local neutrality holds and thus $n_c = n$.

Motivated by $LiFePO_4$,[20,37,39–41] consider a regular solution model[16,49,90] for the reduced state R =Li with mole fraction c,

$$\mu_{Li} = k_B T \ln \frac{c}{1-c} + \Omega(1-2c) \tag{47}$$

where the first term is the configurational entropy and the second the enthalpy of mixing (setting $\mu = 0$ at half filling as a reference). The Nernst potential (Eq. (24)) is

$$\Delta\phi(c) = \Delta\phi^0 - \frac{\mu_{Li}(c)}{e} + \frac{k_B T}{e} \ln a_e(c) \tag{48}$$

and, for insertion at the cathode, the open circuit voltage of the battery is $V_O(c) = \Delta\phi(c) - \Delta\phi_{anode}$. Suppose the transition state excludes s sites (where $s > 1$ accounts for the Li^+ solvation shell) and has reorganization energy λ_0, so that Eq. (46) implies $E\ddagger = \frac{\lambda_0}{4}$ in Eq. (13). The exchange current Eq. (28) then takes the form,

$$I_0(c) = eA(a_+ a_e(c))^{1-\alpha} c^{\alpha} (1-c)^{s-\alpha} \exp\left(\frac{4\alpha\Omega(1-2c) - \lambda_0}{4k_B T}\right) \tag{49}$$

where a_+ is the Li^+ activity in the electrolyte.

This example illustrates how our theory unifies charge-transfer reaction kinetics, equilibrium thermodynamics, and ion transport in a single thermodynamic framework. In contrast, existing porous electrode theories for Li-ion batteries[5,10,11,13] contain thermodynamic inconsistencies. Doyle et al.[10] assume the rate expression Eq. (2) for polymer insertion,[91] which corresponds to Eq. (49) with $a_+ = a_e = 1$, $\Omega = 0$, and $s = 1$ (with $\alpha_c = \alpha$ and $\alpha_a = 1 - \alpha$ also reversed). The electrolyte activity a dilute solution, $a_+ = c_+$ has also been included,[13] but all of these models are inconsistent with the use of concentrated solution models($a_+ \neq c_+$) to fit experimental data. Another common inconsistency is that the open circuit voltage, $V_O(c)$, is fitted independently, when it should be related to the local activities of ions in solid solution Eq. (47) in both the Nernst equation, Eq. (48), and the exchange current density, Eq. (49). It is also inconsistent to model solid diffusion by Fick's law with a fitted nonlinear diffusivity, rather than using ionic activity gradients in Eq. (4), consistent with $V_O(c)$ and $I_0(c)$.

Semiconducting insertion electrodes. The electron activity, $a_e(c)$, generally depends on the local ion concentration. This effect is often negligible in mixed ion-electron conductors with $a_e \approx 1$, but it is important in semiconducting insertion electrodes with poor intrinsic electron

conductivity. Important examples include amorphous silicon (a-Si), a high-energy-density anode material,[46,92,93] and tungsten bronze (Li_cWO_3), an electrochromic material.[94–96] Since Li acts as an electron donor impurity, the density of free electrons increases with lithium filling as $\rho_e = \rho_e^0 + c\rho_s p_d$, where ρ_s is the density of intercalation sites, and p_d is the probability that Li donates a delocalized electron to the conduction band. Assuming a simple free electron model in d dimensions, the electron activity is given by

$$a_e(c) \propto \exp\left(\frac{E_f(c)}{k_B T}\right), \tag{50}$$

in terms of the Fermi energy,

$$E_f(c) = \frac{\hbar^2 \alpha_d (\rho_e^0 + c\rho_s p_d)^{2/d}}{2m^*} \tag{51}$$

where m^* is the effective mass of electrons in the conduction band and α_d is a constant ($\alpha_1 = \pi^2$, $\alpha_2 = 2\pi$, and $\alpha_3 = (3\pi^2)^{2/3}$).

There are many interesting cases. For metals, we can set $a_e \approx$ constant, due to the large density of intrinsic electron states, $\rho_e^0 \gg \rho_s$. In the case of an ideal solid solution (Eq. (47) with $\Omega = 0$) in a three-dimensional semiconductor ($\rho_e^0 = 0, d = 3$), we recover the model of Raistrick and Huggins[49,96] for the open circuit voltage of Li_cWO_3 using Eq. (50) and Eq. (51) in the Nernst equation Eq. (48). In contrast to prior Butler-Volmer models of coloration dynamics in tungsten bronze,[94,95] however, our theory shows how to consistently formulate insertion kinetics (Eq. (49)) and transport (Eq. (4)). The theory also predicts different lithium concentration dependence for electrode kinetics in anisotropic low-dimensional electron conductors, such as graphene flakes ($d = 2$) and silicon or carbon nanotubes ($d = 1$), which are increasingly used in battery electrodes.[46,93]

In the preceding analysis, we have neglected diffuse charge (or space charge) in the solid, which is valid only once the doping by ion insertion has moved the Fermi level well into the conduction band ($\Delta E \gg k_B T$). In a more general treatment of the depleted/insulator state, intercalated ions and/or electron holes at potential ϕ_e also participate in the reaction (Figure 2(a)). However, this

requires also describing electrostatics and transport (via Poisson-Nernst-Planck equations) in the electrode and electrolyte phases, as outlined below, and results in Frumkin corrections to Butler-Volmer kinetics.[88,89]

Solid oxide electrocatalysis. To illustrate the theory for a multistep reaction, consider the oxygen reduction reaction, $O_{2(g)} \rightarrow 2O^{2-}_{(s)}$, at the cathode of a solid oxide fuel cell (SOFC) (Figure 4(c)). Oxygen gas adsorption on the electrode catalyst, e.g. lanthanum strontium manganite (LSM) is followed by two charge transfer steps and ion intercalation in the solid oxide electrolyte, e.g. yttrium stabilized zirconia (YSZ) .[22,97–100] (Similar concepts could be applied to multi-step hydrogen oxidation at the anode.[101]) Assuming a Langmuir isotherm for surface adsorption and Nernst equations for charge transfer, equilibrium conditions for the three steps are:

$$\text{Step 1:} \quad \mathrm{O}_{2(g)} \rightarrow 2\mathrm{O}_{ads}, \qquad a_{O_2} = Kp_{O_2} = a_O^2 = \left(\frac{\Theta_O}{1-\Theta_O}\right)^2 \tag{52}$$

$$\text{Step 2:} \quad \mathrm{O}_{ads} + e^- \rightarrow \mathrm{O}^-_{(s)}, \quad \Delta\phi_2^{eq} = \Delta\phi_2^0 + \frac{k_BT}{e}\ln\frac{a_O a_e}{a_{O^-}} \tag{53}$$

$$\text{Step 3:} \quad \mathrm{O}^-_{(s)} + e^- \rightarrow \mathrm{O}^{2-}_{(s)}, \quad \Delta\phi_3^{eq} = \Delta\phi_3^0 + \frac{k_BT}{e}\ln\frac{a_{O^-} a_e}{a_{O^{2-}}} \tag{54}$$

where p_{O_2} is the partial pressure of oxygen. The theory can be applied to each step, but let us assume that step 2 is rate limiting. In that case, the first charge transfer sustains the over potential, $\eta = \Delta\phi - \Delta\phi_2^{eq}$, while the second is in equilibrium, $\Delta\phi = \Delta\phi_3^{eq}$.

Assuming s excluded sites in the transition state and plugging Θ_O into Eq. (13), we obtain a Butler-Volmer equation for step 2,

$$I = \left[\frac{\nu e A e^{-E_\ddagger/k_BT}\left(a_e\sqrt{Kp_{O_2}}\right)^{1-\alpha} a_{O^-}^{\alpha}}{\left(1+\sqrt{Kp_{O_2}}\right)^s}\right]\left(e^{-\alpha e\eta/k_BT} - e^{(1-\alpha)e\eta/k_BT}\right) \tag{55}$$

The equilibrium conditions for steps 1 and 3 determine the intermediate activity a_{O^-}, which can be be eliminated in Eq. (55) to obtain a Butler-Volmer equation for the net reaction,

$$I = \left[\frac{\nu e A e^{-E'_\ddagger/k_BT}\left(Kp_{O_2}\right)^{(2-\alpha)/4} a_e^{1-\alpha} a_{O^{2-}}^{\alpha/2}}{\left(1+\sqrt{Kp_{O_2}}\right)^s}\right]\left(e^{-\alpha e\eta/2k_BT} - e^{(2-\alpha)e\eta/2k_BT}\right) \tag{56}$$

where $E'_{\ddagger} = E_{\ddagger} + \frac{\alpha}{2}(\Delta\phi_3^0 - \Delta\phi_2^0)$. The exchange current has the typical "volcano" dependence of electrocatalysis: The rate increases with Kp_{O_2} at low pressure and small adsorption energy, $E_a = k_B T \ln K$, as $(Kp_{O_2})^{(2-\alpha)/4}$, but then decreases at high pressure or high adsorption energy due to surface saturation, as $(Kp_{O_2})^{-s/2}$. For $\alpha = \frac{1}{2}$ and $s = 1$, the scaling exponents are $\frac{3}{8}$ and $-\frac{1}{2}$, respectively. The cathodic transfer coefficient is $\alpha_c = \alpha/2$, so, even if the rate limiting step is symmetric ($\alpha = \frac{1}{2}$), the net reaction appears to be asymmetric ($\alpha_c = \frac{1}{4}$) .[4,5]

Ionic liquids. As in ionic crystals, crowding effects are also important in solvent-free ionic liquids. Important examples include molten salts in liquid metal batteries[102] and aluminum smelting[103] and room-temperature ionic liquids (RTIL) in chemical synthesis[104] and capacitive energy storage.[105,106] In spite of liquid disorder, solid-solution models for the configurational entropy have been applied to RTIL,[30,34,107] in which case Faradaic reactions could be described by the models above for ion intercalation in crystals. It is more natural to consider hard-sphere liquid models,[26,28,29,108,109] although such models lose accuracy in highly charged double layers.[26,110]

For identical hard spheres, the Carnahan-Starling equation of state[111] (valid up to $\approx 55\%$ volume fraction) corresponds to the excess chemical potential,

$$\frac{\mu_i^{ex}}{k_B T} = \ln \gamma_i = \frac{\Phi(8 - 9\Phi + 3\Phi^2)}{(1-\Phi)^3} \tag{57}$$

which may be suitable for entropic effects in simple, high-temperature molten salts, such as NaCl. For RTILs, which often have very different ion sizes, the extension for non-identical hard-sphere mixtures[112,113] yields the following chemical potential of species i in a mixture of N species with diameters $\{a_i\}$:

$$\begin{aligned} \ln \gamma_i &= -\left(1 + \frac{2\xi_2^3 a_i^3}{\Phi^3} - \frac{3\xi_2^2 a_i^2}{\Phi^2}\right)\ln(1-\Phi) + \frac{3\xi_2 a_i + 3\xi_1 a_i^2 \xi_0 + a_i^3}{1-\Phi} \\ &+ \frac{3\xi_2 a_i^2}{(1-\Phi)^2}\left(\frac{\xi_2}{\Phi} + \xi_1 a_i\right) - \xi_2^3 a_i^3 \frac{\Phi^2 - 5\Phi + 2}{\Phi^2(1-\Phi)^3} \end{aligned} \tag{58}$$

where $\xi_n = \sum_{j=1}^N \Phi_j a_j^{n-3}$, Φ_j is the volume fraction of species j, and $\Phi = \sum_{j=1}^N \Phi_j$ is the total

volume fraction of ions. If we assume that s times the volume of the active ion of species i is excluded in the transition state,

$$\gamma_{\ddagger} = \gamma_i^s e^{4\lambda_0/k_BT}, \tag{59}$$

then the exchange current for the Faradaic reaction, $O_i + e^- \rightarrow R_j$ (converting species i to j) is given by Eq. (28) with γ_i and γ_j from Eq. (57). This approach may give insights into the relative reactivity of ions of different sizes. Without a polar solvent, the reorganization energy λ_0 is smaller and can be comparable to k_BT, so asymmetric ($\alpha \neq \frac{1}{2}$) and multiple electron transfer ($n > 1$) may be possible, especially in molten salts at high temperature.

Phase-Field Theory of Electrode Kinetics

Bulk phase-field models. In a continuous, homogeneous, open system at constant pressure and temperature, the diffusional chemical potential is the derivative of the free energy with respect to composition. More generally, the it is the variational derivative of the free energy functional $F[c]$, which is the continuum analog of adding a particle and allowing the system to relax, e.g. by removing a vacancy in a crystal. To describe the free energy of an inhomogeneous system, Van der Waals[114] added the "gradient energy" to the bulk integral over the volume V,

$$F[c] = \int_V \left[\rho_s \bar{f}(c) + \frac{1}{2} \nabla c \cdot \kappa \nabla c \right] dV \tag{60}$$

where κ is the symmetric, positive definite, "gradient penalty tensor". For intercalation phenomena, we define the (Helmholtz) free energy $\bar{f}$ and filling fraction c per crystal site, so we multiply by the site density ρ_s to obtain the free energy per volume. The second integral is over the surface S with surface tension γ_s depending on the normal orientation $\hat{n}$. The chemical potential is given by

$$\mu = \frac{1}{\rho_s} \frac{\delta F}{\delta c} = \bar{g}'(c) - \frac{\nabla \cdot \kappa \nabla c}{\rho_s} \tag{61}$$

which depends on the curvature of the concentration profile.

This formulation of non-equilibrium thermodynamics was introduced in materials science by Cahn and Hilliard (CH) in 1958[90,115–117] and forms the basis for modern phase field models.[16] (In physics, similar models were introduced by Landau for second-order phase transitions[118] and Ginzburg and Landau for superconductivity.[119]) The gradient energy can be justified as the first term in the Taylor expansion of a nonlocal inhomogeneous free energy around the homogeneous state. If $\bar{f}(c)$ has multiple minima representing distinct stable phases, then the gradient term counteracts the tendency to phase separate and leads to a diffuse interface of width λ, whose concentration profile solves the Beltrami equation, $\mu =$ constant. In that case, we can also relate κ to the inter-phasial tension, γ_i.

Toward an electrochemical phase-field theory. Building on earlier models of phase separation in ionic systems,[120–122] there were several breakthroughs in 2004 that set the stage for my theory of electrochemical kinetics. Garcia, Bishop and Carter[19] formulated variational principles for electromagnetically active systems, which unify the CH equation with Maxwell's equations. In the same year, Guyer, Boettinger, Warren and McFadden[17,18] introduced phase-field models to electrochemistry by representing a diffuse electrode/electrolyte interface with a continuous phase field, $\xi(x)$, varying between stable values 0 and 1. As in phase-field models of dendritic solidification,[84–87] they used Landau's quartic model, $\bar{f}(\xi) \propto \xi^2(1-\xi)^2$, to provide a double-welled homogeneous free energy ($c = \xi$ in Eq. (60)) to separate the electrolyte and electrode phases. They described the kinetics of electrodeposition[18] (converting ions in the electrolyte to solid metal) by Allen-Cahn kinetics,[123] linear in the thermodynamic driving force, $I \propto \Delta\mu$, but did not make connections with the Butler-Volmer equation or charge-transfer theory. Several groups have used this approach to model dendritic growth.[81–83]

Also in 2004, Han, Van der Ven and Ceder[20] first applied the CH equation to the diffusion of intercalated lithium ions in LFP, albeit without modeling reaction kinetics. Following Cahn and Hilliard[90], they used the regular solution model (Eq. (47)) with homogeneous free energy,

$$\bar{f}(c) = k_B T\left[c\ln c + (1-c)\ln(1-c)\right] + \Omega c(1-c) \tag{62}$$

where the terms (from left to right) represent the entropy of particles, the entropy of holes, and the enthalpy of particle-hole interactions. At high temperature, entropy dominates, and there is only one minimum at $c = \frac{1}{2}$ with maximal mixing. If $\Omega > 0$, then particles attract each other (and repel holes), and, below a critical temperature, $T < T_c = \frac{\Omega}{2k_B}$, there are two minima representing stable high-density and low-density phases, separated by a miscibility gap, or voltage plateau.[25,40] Balancing terms in Eq. (60), the phase boundary width scales as $\lambda_i \approx \sqrt{\kappa/\Omega}$, and the inter-phasial tension as $\gamma_i \approx \sqrt{\kappa\Omega}\rho_s$.[16,39,90]

These developments, followed by the observation of phase boundaries at LFP surfaces,[67,124] led to the first phase-field theory of Faradaic reactions. The exponential (Tafel) dependence of the current on the overpotential, defined in terms of $\Delta\mu$ in Eq. (61), was first reported in 2007,[36,37,125] but with a spurious pre-factor, noted by Burch.[39,66] The complete theory, connecting the CH model to the BV equation and the battery voltage, appeared in 2009[35,71] and later applied to LFP nanoparticles.[40,41] For lithium intercalation, the reduced state has zero charge ($z_R = 0$), so the original CH functional Eq. (60) with $\bar{f}(c)$ given by Eq. (47) was used to construct the electrochemical potential Eq. (61) in the Butler-Volmer and Nernst equations.

Variational formulation of electrode kinetics. For electrochemical kinetics, we consider the total Gibbs free energy G of an open system, where the electrochemical potential is related to the cell voltage. For the general Faradaic reaction (Figure 2),

$$O + ne^- = \sum_i s_i O_i^{z_i} + ne^- \rightarrow \sum_j s_j R_j^{z_j} = R, \tag{63}$$

we define all the chemical activities a_k and diffusional electrochemical potentials μ_k variationally:

$$\mu_O = k_B T \ln a_O + z_O e\phi_O = \sum_i \frac{s_i}{\rho_s}\frac{\delta G}{\delta c_i} \tag{64}$$

$$\mu_R = k_B T \ln a_R + z_R e\phi_R = \sum_j \frac{s_j}{\rho_s}\frac{\delta G}{\delta c_j} \tag{65}$$

$$\mu_e = k_B T \ln a_e - e\phi_e = \frac{1}{\rho_s}\frac{\delta G}{\delta c_e} \tag{66}$$

The Nernst voltage $\Delta\phi^{eq}$ is defined variationally by setting $\mu_R = \mu_O + n\mu_e$. According to Eq. (24), Eq. (25) and Eq. (34), the activation overpotential

$$\eta = \Delta\phi - \Delta\phi^{eq} = \phi_e - \phi - \frac{k_B T}{n_c e} \ln \frac{a_e^n a_O}{a_R} = \frac{\mu_R - (\mu_O + n\mu_e)}{ne} = \frac{\mu_2 - \mu_1}{ne} \tag{67}$$

is the change in *total* chemical potential of the Faradaic reaction per charge transferred ($n_c = n$). In this way, the diffusional electrochemical potentials $\mu_i = \frac{\delta G}{\rho_s \delta c_i}$ enter the Butler-Volmer (Eq. (1)) and Marcus (Eq. (40)) equations, as well as the exchange current Eq. (28).

The following free energy captures the essential physics of ionic materials:[17,19,34,37,39–41,43]

$$G = \int_V \left[\rho_s \left(\bar{f}(\vec{c}) + \rho_e \phi \right) + \frac{1}{2} \left(\nabla \vec{c} \cdot \kappa \nabla \vec{c} - \nabla \phi \cdot \varepsilon_p \nabla \phi + \sigma : \varepsilon \right) \right] dV + \oint_S \gamma_s(\hat{n}, \vec{c}, \phi) dS \tag{68}$$

where $\vec{c}$ is the set of concentrations, ε_p the permittivity tensor, κ the gradient penalty tensor, σ the stress tensor, ε the strain tensor, q_s the surface charge density, and $\rho_e = \sum_i z_i e c_i$ the bulk charge density (for ions and electrons, in the case of mixed conductors). The electrostatic potential acts as a Lagrange multiplier controlling the total ion densities[19,41] while enforcing Maxwell's equations. (See also the supporting material of Bazant et al.[34]).

Mechanical deformation due to inserted ions can significantly affect charge-transfer kinetics.[41] Assuming linear elasticity, the stress is given by Hooke's law, $\sigma_{ij} = C_{ijkl}\varepsilon_{kl}$, where C is the elastic constant tensor. The lattice-preserving "coherency strain",

$$\varepsilon_{ij} = \frac{1}{2} \left(\frac{\partial u_i}{\partial x_j} + \frac{\partial u_j}{\partial x_i} \right) - \sum_m \varepsilon_{ijm}^0 c_m \tag{69}$$

is the total strain due to compositional inhomogeneity (first term) relative to the stress-free inelastic strain (second term). In a mean-field approximation (Vegard's law), each molecule of species m exerts an independent strain ε_m^0 (lattice misfit between $c_m = 0, 1$).

In our theory, *the Nernst voltage Eq.* (24) *and exchange current Eq.* (28) *depend on concentra-*

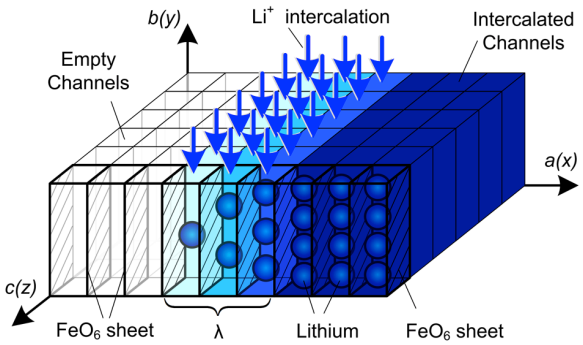

Figure 5: Insertion kinetics in LFP nanoparticles. The low-energy phase boundary between $FePO_4$ and $LiFePO_4$ propagates as an "intercalation wave"[37,40,41,52,125] across the {010} facet, filling the crystal layer by layer, where the reaction rate (Eq. (72)) is enhanced by concentration gradients and elastic stress. [Reproduced from Bai, Cogswell, Bazant.[40]]

tion gradients and elastic stress via,

$$\mu_i = \frac{\delta G}{\rho_s \delta c_i} = \left(\frac{\partial \bar{f}}{\partial c_i} + \frac{\nabla \cdot \kappa \nabla c_i - \sigma : \varepsilon_i^0}{\rho_s} \right) + z_i e \phi = k_B T \ln a_i + z_i e \phi \tag{70}$$

which leads new modes of ion intercalation (Figure 5). For ion insertion (Figure 3), we propose the general model,

$$\gamma_\ddagger = (1 - c_i)^{-s} \exp\left[\frac{1}{k_B T} \left(\frac{\lambda_0}{4} - \frac{\sigma : \varepsilon_\ddagger}{\rho_s} \right) \right] \tag{71}$$

where $\varepsilon_\ddagger$ is the transition-state strain, $s \geq 1$ the number of excluded sites, and λ_0 the reorganization energy. For insertion in a regular solid solution, the exchange current is

$$I_0 = \bar{I}_0(c) \exp\left(\frac{\alpha(\nabla \cdot \kappa \nabla c) + \sigma : (\varepsilon_\ddagger - \alpha \varepsilon^0)}{\rho_s k_B T} \right) \tag{72}$$

where $\bar{I}_0(c)$ is the limit of zero stress and uniform concentration Eq. (49) and $\Delta\varepsilon = \varepsilon_\ddagger - \alpha\varepsilon^0$, is the "activation strain".[126]

Conservation laws. From the LIT flux Eq. (4), conservation of mass leads to the CH equation,

$$\frac{\partial c_i}{\partial t} + \nabla \cdot \mathbf{F}_i = \bar{R}_i, \tag{73}$$

where,

$$\mathbf{F}_i = -\frac{D_i c_i}{k_B T \rho_s} \nabla \frac{\delta G}{\delta c_i} \tag{74}$$

In our formulation, the tracer diffusivity D_i is also defined variationally via Eq. (15). In the case of a solid solution, Eq. (16), this leads to the "modified CH equation".[79] The homogeneous reaction rate $\bar{R}_i$, describing bulk charge transfer reactions (e.g. water self-ionization), is often neglected, but could be described by our theory. The current density is also expressed variationally:

$$\mathbf{J} = \sum_i z_i e \mathbf{F}_i \tag{75}$$

and enters charge conservation,

$$\frac{\partial \rho_e}{\partial t} + \nabla \cdot \mathbf{J} = \sum_i z_i e \bar{R}_i = 0. \tag{76}$$

Since elastic stress relaxes much faster than diffusion, mechanical equilibrium $\frac{\delta G}{\delta \vec{u}} = 0$ implies $\nabla \cdot \boldsymbol{\sigma} = 0$.

Since the chemical potential involves two spatial derivatives (Eq. (61)), the CH equation is fourth-order and requires two boundary conditions at each interface. One relates the normal flux to the reaction rate

$$\hat{n} \cdot \mathbf{F}_i = R_i \tag{77}$$

where $R_i = 0$ for an inactive species and $R_i = \frac{J}{s_i z_i e}$ for an active species. The other is the "variational boundary condition",

$$[\hat{n} \cdot \boldsymbol{\kappa} \nabla c_i] = \frac{\partial \gamma_s}{\partial c_i} \tag{78}$$

(where [X] denotes the jump in X at an interface), which ensures continuity of the chemical potential[39] and controls surface wetting and nucleation.[40]

Electrostatics. In most models of electrochemical systems, the potential ϕ is determined implicitly by electroneutrality, $\rho_e = 0$, but here we allow for diffuse charge, which can alter reaction

rates (the “Frumkin correction" below) and contribute to capacitive charge storage. The mean electrostatic potential ϕ in Eq. (68) is uniquely defined at each position in the microstructure. The potentials ϕ_O, ϕ_R and ϕ_e refer to ϕ on appropriate sides of the interface where a Faradaic reaction occurs (Figure 2).

The potential is determined variationally by $\frac{\delta G}{\delta \phi} = 0$. Bulk variations lead to Poisson's equation,

$$\nabla \cdot \mathbf{D} \equiv -\nabla \cdot (\varepsilon_p \nabla \phi) = \rho_e \tag{79}$$

and surface variations to the electrostatic boundary condition,

$$[\hat{n} \cdot \mathbf{D}] \equiv -[\hat{n} \cdot \varepsilon_p \nabla \phi] = \frac{\partial \gamma_s}{\partial \phi} \equiv q_s \tag{80}$$

where q_s is the surface charge (per area), $\mathbf{D} = \varepsilon_p \cdot \mathbf{E}$ is the Maxwell displacement field and $\mathbf{E} = -\nabla \phi$ is the electric field. For ionic liquids, higher-order terms, such as $(\nabla^2 \phi)^2$, can be added to the free energy density to describe electrostatic correlations, and ε_p becomes a differential operator.[34]

Since the surface charge q_s is not fixed at an electrode surface, another boundary condition is needed for Poisson's equation Eq. (79), which relates the charge to the interfacial voltage $\Delta\phi = [\phi]$. In electrochemistry, it is usually assumed that $\Delta\phi$ is across the entire double layer, but as emphasized by Frumkin long ago,[127] the diffuse part of the double layer outside the reaction plane must be excluded. Mathematical models of the Frumkin correction have recently been developed for solid electrolytes,[128–130] liquid electrolytes[88,130–132] and porous electrodes[133–135] (See Biesheuvel et al.[130] for a review.) Assuming that charge transfer occurs across a charge-free layer of thickness h_s and permittivity ε_s with constant electric field $\Delta\phi/h_s$, which could represent a Stern layer of electrode solvation[88] or the radius of an ionic liquid molecule,[34] the continuity of Maxwell displacement implies

$$\Delta\phi = \lambda_s \hat{n} \cdot \nabla \phi \tag{81}$$

where $\lambda_s = h_s \varepsilon_p / \varepsilon_s$ is an effective thickness of the Stern layer. The role of diffuse charge is con-

trolled by dimensionless parameter, $\delta_s = \lambda_s/\lambda_D$, where λ_D is the Debye screening length:[88,130,132,134] In the Helmholtz limit ($\delta_s \to 0$), the double-layer is compact (at the molecular scale), and standard BV kinetics apply; in the Gouy-Chapman limit ($\delta \to \infty$) it is diffuse and acts like a semiconductor diode, where forward (or reverse) bias corresponds to electrostatic condensation (or repulsion) of the active ions.

Ion Intercalation with Phase Separation

Size-dependent solubility. It is well known that the spinodal gap of unstable compositions in a solid solution shrinks with decreasing particle size,[117] as low energy long-wavelength fluctuations are prohibitted. The miscibility gap also shrinks, since the relative cost of a phase boundary increases with the surface to volume ratio.[136] Elastic coherency strain enhances both effects by increasing the energy penalty for phase separation.[41,54,59]

The theory predicts novel effects of *kinetics* on solubility, due to ion exchange with the electrolyte reservoir.[39,41] At constant voltage, the spinodal and miscibility gaps shrink with increasing exchange current,[39] since fluctuations with fast reactions promote unfavorable concentration gradients. Experimental solubility data[56] can be interpreted using a 1D Cahn-Hilliard-reaction (CHR) model,[39,66] or a more accurate, 2D reaction-limited model with coherency strain.[41]

Intercalation waves. In anisotropic crystals, ion intercalation dynamics can be limited by diffusion or reactions, independently in each direction.[37] In LFP nanoparticles, the concentration tends to remain uniform in the [010] direction due to the fast diffusion[57,137] and elastically unfavorable phase separation[41] in short one-dimensional channels, unblocked by Fe anti-site defects.[58] After [010] depth-averaging,[37] the full CHR model reduces to a new, reaction-limited model on the active $\{010\}$ crystal facet,

$$\frac{\partial c}{\partial t} = J_0 f(\eta), \tag{82}$$

(where $J_0 = I_0/A_s$ is the current per surface site), which is an electrochemical generalization of the Allen-Cahn equation[16,123] (EAC) with with a nonlinear dependence on the variational overpoten-

tial,

$$\eta = \frac{1}{e\rho_s}\frac{\delta G}{\delta c} + \Delta\phi, \tag{83}$$

where $f(\eta) = I/I_0$ can come from the BV (Eq. (1)) or Marcus (Eq. (40)) equations. For lithium insertion in a regular solution,[40,41] the exchange current $I_0(c, \nabla\cdot\kappa\nabla c, \sigma)$ is given by Eq. (72).

The theory has led to a paradigm shift in understanding insertion dynamics. In contrast to prior battery models, which assume a uniform reaction rate over the particle surface, limited by radial solid diffusion[10,11,138] or a shrinking-core phase boundary,[12,13] the EAC limit of the CHR model predicts reaction-limited intercalation waves (or "domino cascades"[139]), sweeping across the active facet, filling the crystal layer by layer (Figure 5) .[37,40,41,125,140] Intercalation waves result from nucleation at surfaces or defects, or by spinodal decomposition,[40] and trace out the voltage plateau at low current, as shown in Figure 6. Experimental evidence of one-dimensional nucleation and growth, consistent with the EAC theory,[37,40] has recently been obtained by potentiostatic intermittent titration.[63]

Suppression of phase separation and quasi-solid solution. The theory has led to some surprising conclusions about *electrochemically driven phase transformations*. Our first paper included a mathematical proof that traveling-wave solutions of the EAC equation only exist over a finite range of thermodynamic driven force,[36,37] but the implications were difficult to grasp without the connection to the battery voltage. Once the generalization of BV kinetics was achieved,[35,71] simulations and analysis revealed how phase separation is strongly influenced by the applied current.[40,41] As suggested by Malik et al.[55] based on bulk equilibrium free energy calculations, phase separation is suppressed during battery operation, but we now understand that the mechanism is due to surface reactions, far from equilibrium.

As explained by Bai et al.[40], phase separation is suppressed, when the applied current approaches the exchange current. A linear stability analysis of the EAC model for BV kinetics with $\alpha = \frac{1}{2}$ shows that concentration fluctuations of wavenumber k grow at a rate[40]

$$s(k;c,I) = -\sqrt{\bar{J}_0 + \frac{I^2}{4}}(\bar{\eta}' + \kappa k^2) + I\left(\frac{\bar{J}_0'}{\bar{J}_0} + \frac{1}{2}\kappa k^2\right) \tag{84}$$

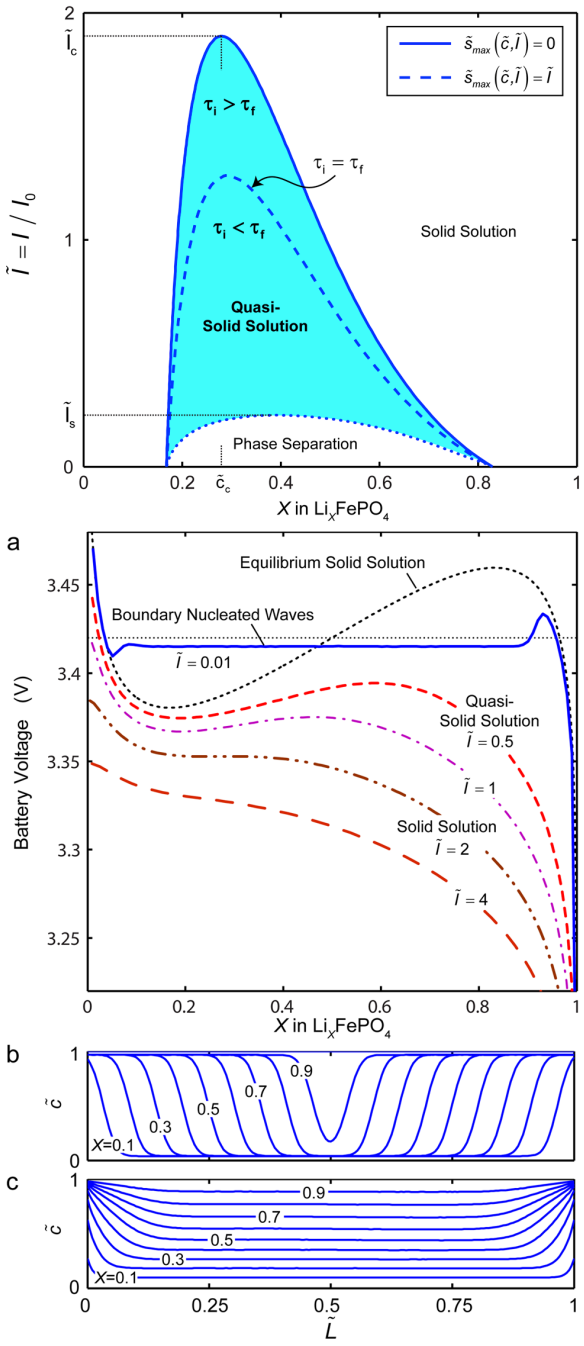

Figure 6: Galvanostatic discharge into a single LFP cathode nanoparticle without coherency strain. Top: Linear stability (spinodal) diagram for the homogeneous state versus current $\tilde{I}$ (scaled to the exchange current at $X = 0.5$) and mean Li filling X. (a) Battery voltage versus state of charge (X) at different currents $\tilde{I}$. (b) Evolution of the concentration profile at low current $\tilde{I} = 0.01$ with insertion waves nucleated at the wetted [001] side facets. (c) Quasi-solid solution behavior close to the critical current $\tilde{I} = 0.5$, showing homogeneous filling ahead of the waves. [Reproduced from Bai, Cogswell, Bazant[40]]

where $\bar{\eta}(c)$ and $\bar{J}_0(c)$ are the activation overpotential and exchange current density, respectively, in a homogeneous state of concentration c sustaining a current I. The range of linear instability, $s(c,I) > 0$, predicted by Eq. (84) and Eq. (72) with elastic strain is shown in Figure 6(a).

The theory predicts a *critical current*, of order the exchange current, above which phase separation by spinodal decomposition is impossible. Below this current, the homogeneous state is unstable over a range of concentrations (smaller than the zero-current spinodal gap), but for large currents, the time spent in this region is too small for complete phase separation. Instead, the particle passes through a transient *quasi-solid solution* state, where its voltage and concentration profile resemble those of a homogeneous solid solution.

The suppression of phase separation predicted by the theory is very general. When nucleation is possible (see below), a similar current dependence is observed. As shown in Figure 6, the bulk crystal fills ahead of the surface-nucleated intercalation waves in the quasi-solid solution regime, while homogeneous filling occurs above the critical current. With elastic coherency strain included, the suppression of phase separation is analogous, but even stronger.[41]

In the case of LFP, the critical current is an order of magnitude smaller than the exchange current.[41] The surprising implication is that phase separation does not occur *in situ* during normal battery operation, which helps to explain the high-rate capability and extended lifetime of LFP nanoparticles, due to larger active area and smaller elastic stresses. On the other hand, phase separation occurs at very low currents and can be observed in particles trapped at intermediate compositions for *ex situ* measurements (Figure 7).

Striped phase morphologies. For quantitative interpretation of experiments, it is essential to account for the elastic energy. Even a simple elastic model can dramatically improve the inference of lithium diffusivity from intermitted titration with phase separation.[141] Crystal anisotropy generally leads to striped patterns in equilibrium.[41,43,59,60] Cogswell and Bazant[41] showed that the stripe spacing

$$\lambda_{stripe} = \sqrt{\frac{2\gamma_i L}{\Delta g}} \tag{85}$$

follows from the balance between elastic energy, favoring short wavelengths at a stress-free bound-

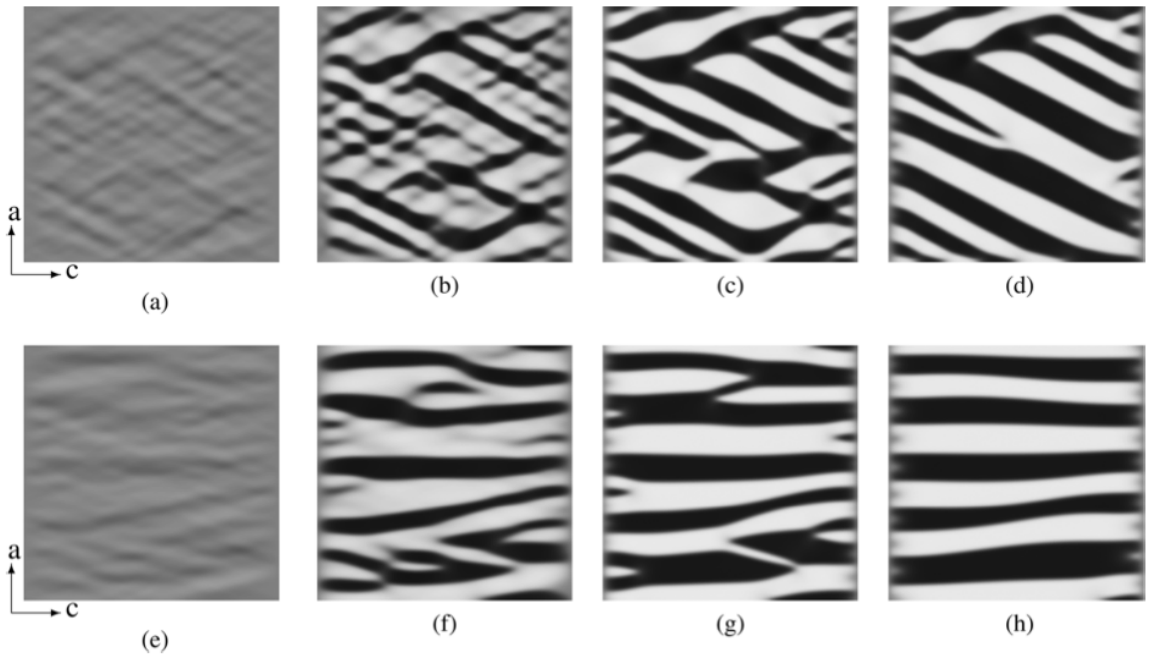

Figure 7: Simulations of reaction-limited phase separation of a 500nm single crystal of $Li_{0.5}FePO_4$ into Li-rich (black) and Li-poor phases (white) in an electrolyte bath at zero current and zero pressure, consistent with *ex situ* experiments.[67,124,142] (a) Coherent phase separation, where lithium insertion causes contraction along [001] (*c*) axis and expansion along the [100] (*a*) axis, leading to tilted interfaces aligned with {101} planes. (b) Loss of [001] coherency (e.g. due to microcracks[67]) causes the phase boundaries to rotate to align with {100} planes. [Reproduced from Cogswell and Bazant[41].]

ary, and interfacial energy, favoring long wavelengths to minimize interfacial area. (Here, Δg is the free energy difference between the homogeneous and phase separated states, and L is the particle size.)

In layered crystals, the lattice misfit can cause tension and compression in different directions, and Stanton and Bazant[43] predicted that this could cause phase boundaries to tilt with respect to the crystal axes. For example, lithium insertion in LFP causes contraction of the iron phosphate planes in the [001] direction and expansion in the [100] and [010] directions.[67] Cogswell quantitatively explained the experimentally observed phase morphologies[124,142] and used the theory (Eq. (85)) to extract γ_i and thus the gradient penalty κ. As shown in Fig. Figure 7, the new phase-field theory enables realistic simulations of reaction-limited phase separation for single particles at zero total current.

Surface wetting and nucleation. The theory also predicts how *surface thermodynamics affects reaction kinetics*. We have already mentioned the Frumkin effect of electrostatic amplification of the reaction rate, when active ions are attracted to the surface. Non-electrostatic attraction, or *wetting*, of the solid surface by intercalated ions can also dramatically affect the intercalation process. In Cahn's theory,[143] surface wetting is described by Eq. (78) with $\frac{\partial \gamma_s}{\partial c} < 0$. Using this boundary condition for the EAC equation Eq. (82), the nucleation of intercalation waves in LFP nanoparticles due to wetting of the $\{100\}$ crystal facet can be simulated with coherency strain [41] (Figure 7) or without[40] (Figure 6). By combining surface wetting with elastic strain in the theory, the nucleation barrier in LFP (critical voltage past the equilibrium plateau to observe a sudden current) can be predicted as a function of particle size, in excellent agreement with experiments. The effect of surface wetting on intercalation kinetics may also be responsible for the surprising performance boost from phosphate-glass thin films on active nanoparticles of LFP [53] and Li_xCoO_2 [144]

Mosaic Instability. The complex dynamics of ion intercalation in nanoparticles also affects the macrosopic response of a composite electrode. Using the CHR model[39] for a collection of particles in a reservoir of constant chemical potential, Burch[66] discovered what we called the mosaic instability, whereby particles filling uniformly at constant total current suddenly fill one-by-one. The mechanism is simple: As the particles enter the miscibility gap, the first to phase separate (due to random nucleation or spinodal decomposition) will suddenly lower its chemical potential and sustain a much larger current until it becomes full, at which point the current is shared by the others until the process repeats. Interestingly, in the CHR model, the smaller particles transform first, because diffusion brings the core concentration to the spinodal more quickly. In contrast, for reaction-limited particles, the larger ones are more likely to nucleate first.

Meanwhile, Dreyer et al.[64] described the mosaic instability and demonstrated it experimentally in two clever ways. They connected it to the zero-current voltage gap between charge/discharge cycles in LFP batteries, as well as the dynamics of an array of balloons connected to a single pressure line. Their theory[64,65] is similar to the "pseudo capacitor limit" of our models, where each particle maintains uniform (but time dependent) concentration, without internal phase separation.

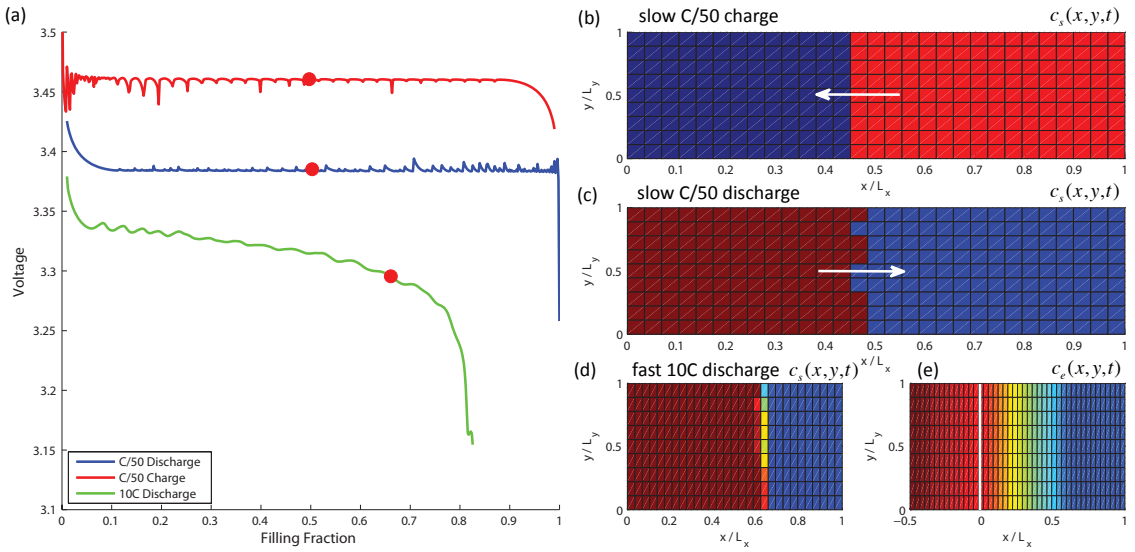

Figure 8: Finite-volume simulations of macroscopic phase separation in a porous LFP cathode.[42] (a) Voltage versus state of charge for slow charge/discharge and fast discharge. (b)-(d) Profiles of mean Li concentration in the solid at the red points in (a), showing narrow reaction fronts with mosaic instabilities, associated with voltage fluctuations. (e) Electrolyte Li concentration for fast discharge (d), showing diffusion limitation. [T. R. Ferguson]

Porous electrodes. The theory has recently been extended to porous electrodes undergoing phase transformations[42] using classical porous electrode models to describe the electrolyte.[145] Diffusion in the electrolyte provides a spatiotemporal bias for the mosaic instability, so that narrow fronts of stochastic particle phase transformations propagate away from the separator (discharge) or current collector (charge) at low current (Figure 8). The width of the reaction front separating low-density and high-density phases increases with current until the entire electrode becomes active, which is a macroscopic analog of the suppression of phase separation in nanoparticles.

The new theory can robustly predict experimental data for phase-separating porous electrodes for the first time without artificially fitting voltage plateaus or enforcing phase boundaries. Using the EAC regular-solution model for LFP[40,41] in a porous electrode,[42] the model can predict tiny voltage oscillations ($< k_BT/e$ =25mV) and the limiting "voltage gap" at very low currents observed in experiments,[64] which give way to a smoothly decaying voltage at high current[53] (Figure 8). Nucleation is also crucial to consider at the porous electrode scale[63] and can be naturally included in theory. Using a two-component regular solution model for graphite intercalation,[35]

the theory is also able to fit experimental data for diffusion-limited intercalation of long graphite anodes[146] with multiple reaction fronts of different colors corresponding to different stages of lithiation.

Conclusion

This Account describes steps to unify chemical kinetics with thermodynamics, electrostatics, and transport in electrochemical systems. The theory has shed light on rate processes in advanced Li-ion batteries with phase-separating nanoparticles. Other applications to energy conversion, such as electrocatalysis in solid oxide fuel cells and charge transfer in ionic liquids, may require incorporating diffuse charge[34,89] and heat transfer[147] in the general framework.

Acknowledgement

This work was supported by the National Science Foundation under Contracts DMS-0842504 and DMS-0948071 and by a seed grant from the MIT Energy Initiative.

References

1. Butler, J. A. V. Studies in heterogeneous equilibria. Part II. The kinetic interpretation of the Nernst theory of electromotive force. *Trans. Faraday Society* **1924**, *19*, 729–733.

2. Erdey-Gruz, T.; Volmer, M. Zur theorie der wasserstoffüberspannung. *Z. Phys. Chem.* **1930**, *150 (A)*, 203–213.

3. Bard, A. J.; Faulkner, L. R. *Electrochemical Methods*; J. Wiley & Sons, Inc.: New York, NY, 2001.

4. Bockris, J. O.; Reddy, A. K. N. *Modern Electrochemistry*; Plenum: New York, 1970.

5. Newman, J. *Electrochemical Systems*, 2nd ed.; Prentice-Hall, Inc.: Englewood Cliffs, NJ, 1991.

6. Kuznetsov, A. M.; Ulstrup, J. *Electron Transfer in Chemistry and Biology: An Introduction to the Theory*; Wiley, 1999.

7. Marcus, R. A. On the theory of oxidation-reduction reactions Involving electron transfer. I. *J. Chem .Phys.* **1956**, *24*, 966–978.

8. Marcus, R. A. . Chemical and electrochemical electron-transfer theory. *Ann. Rev. Phys. Chem.* **1964**, *15*, 155–196.

9. Marcus, R. A. Electron transfer reactions in chemistry. Theory and experiment. *Rev. Mod. Phys.* **1993**, *65*, 599–610.

10. Doyle, M.; Fuller, T. F.; Newman, J. Modeling of Galvanostatic Charge and Discharge of the Lithium/Polymer/Insertion Cell. *Journal of the Electrochemical Society* **1993**, *140*, 1526–1533.

11. Fuller, T.; Doyle, M.; Newman, J. Simulation and optimization of the dual lithium ion insertion cell. *Journal of the Electrochemical Society* **1994**, *141*, 1–10.

12. Srinivasan, V.; Newman, J. Discharge Model for the Lithium Iron-Phosphate Electrode. *Journal of the Electrochemical Society* **2004**, *151*, A1517–A1529.

13. Dargaville, S.; Farrell, T. Predicting Active Material Utilization in $LiFePO_4$ Electrodes Using a Multiscale Mathematical Model. *Journal of the Electrochemical Society* **2010**, *157*, A830–A840.

14. Groot, S. R. D.; Mazur, P. *Non-equilibrium Thermodynamics*; Interscience Publishers, Inc.: New York, NY, 1962.

15. Prigogine, I.; Defay, R. *Chemical Thermodynamics*; John Wiley and Sons, 1954.

16. Balluffi, R. W.; Allen, S. M.; Carter, W. C. *Kinetics of materials*; Wiley, 2005.

17. Guyer, J. E.; Boettinger, W. J.; Warren, J. A.; McFadden, G. B. Phase field modeling of electrochemistry I: Equilibrium. *Phys. Rev. E* **2004**, *69*, 021603.

18. Guyer, J. E.; Boettinger, W. J.; Warren, J. A.; McFadden, G. B. Phase field modeling of electrochemistry II: Kinetics. *Phys. Rev. E* **2004**, *69*, 021604.

19. Garcia, R. E.; Bishop, C. M.; Carter, W. C. Thermodynamically Consistent Variational Principles with Applications to Electrically and Magnetically Active Systems. *Acta Mater.* **2004**, *52*, 11–21.

20. Han, B.; der Ven, A. V.; Morgan, D.; Ceder, G. Electrochemical modeling of intercalation processes with phase field models. *Electrochimica Acta* **2004**, *49*, 4691–4699.

21. Jamnik, J.; Maier, J. Generalised equivalent circuits for mass and charge transport : chemical capacitance and its implications. *Phys. Chem. Chem. Phys.* **2001**, *3*, 1668–1678.

22. Lai, W.; Haile, S. M. Impedance Spectroscopy as a Tool for Chemical and Electrochemical Analysis of Mixed Conductors: A Case Study of Ceria. *J. Amer. Cer. Soc.* **2005**, *88*, 2979–2997.

23. Lai, W.; Ciucci, F. Thermodynamics and kinetics of phase transformation in intercalation battery electrodes Ð phenomenological modeling. *Electrochim. Acta* **2010**, *56*, 531–542.

24. Lai, W.; Ciucci, F. Mathematical modeling of porous battery electrodes - Revisit of Newman's model. *Electrochimica Acta* **2011**, *56*, 4369–4377.

25. Lai, W. Electrochemical modeling of single particle intercalation battery materials with different thermodynamics. *Journal of Power Sources* **2011**, *196*, 6534Ð6553.

26. Bazant, M. Z.; Kilic, M. S.; Storey, B.; Ajdari, A. Towards an understanding of nonlinear electrokinetics at large voltages in concentrated solutions. *Advances in Colloid and Interface Science* **2009**, *152*, 48–88.

27. Bazant, M. Z.; Kilic, M. S.; Storey, B. D.; Ajdari, A. Nonlinear electrokinetics at large voltages. *New Journal of Physics* **2009**, *11*, 075016.

28. Biesheuvel, P. M.; Lyklema, J. Sedimentation–diffusion equilibrium of binary mixtures of charged colloids including volume effects. *J. Phys. Condens. Matter* **2005**, *17*, 6337.

29. Biesheuvel, P. M.; van Soestbergen, M. Counterion volume effects in mixed electrical double layers. *Journal of Colloid and Interface Science* **2007**, *316*, 490–499.

30. Kilic, M. S.; Bazant, M. Z.; Ajdari, A. Steric effects in the dynamics of electrolytes at large applied voltages: I Double-layer charging. *Phys. Rev. E* **2007**, *75*, 021502.

31. Kilic, M. S.; Bazant, M. Z.; Ajdari, A. Steric effects on the dynamics of electrolytes at large applied voltages: II Modified Nernst-Planck equations. *Phys. Rev. E* **2007**, *75*, 021503.

32. Storey, B. D.; Edwards, L. R.; Kilic, M. S.; Bazant, M. Z. Steric effects on ac electro-osmosis in dilute electrolytes. *Phys. Rev. E* **2008**, *77*, 036317.

33. Olesen, L. H.; Bazant, M. Z.; Bruus, H. Strongly nonlinear dynamics of electrolytes in large ac voltages. *Phys. Rev. E* **2010**, *82*, 011501.

34. Bazant, M. Z.; Storey, B. D.; Kornyshev, A. A. Double layer in ionic liquids: Overscreening versus crowding. *Phys. Rev. Lett.* **2011**, *106*, 046102.

35. Bazant, M. Z. *10.626 Electrochemical Energy Systems*; Massachusetts Institute of Technology: MIT OpenCourseWare, http://ocw.mit.edu, License: Creative Commons BY-NC-SA, 2011.

36. Singh, G. K.; Bazant, M. Z.; Ceder, G. arXiv:0707.1858v1 [cond-mat.mtrl-sci].

37. Singh, G.; Burch, D.; Bazant, M. Z. Intercalation dynamics in rechargeable battery materials: General theory and phase-transformation waves in $LiFePO_4$. *Electrochimica Acta* **2008**, *53*, 7599–7613.

38. Burch, D.; Singh, G.; Ceder, G.; Bazant, M. Z. Phase-transformation wave dynamics $LiFePO_4$. *Solid State Phenomena* **2008**, *139*, 95–100.

39. Burch, D.; Bazant, M. Z. Size-dependent spinodal and miscibility gaps for intercalation in nanoparticles. *Nano Letters* **2009**, *9*, 3795–3800.

40. Bai, P.; Cogswell, D.; Bazant, M. Z. Suppression of Phase Separation in $LiFePO_4$ Nanoparticles During Battery Discharge. *Nano Letters* **2011**, *11*, 4890–4896.

41. Cogswell, D. A.; Bazant, M. Z. Coherency strain and the kinetics of phase separation in $LiFePO_4$ nanoparticles. *ACS Nano* **2012**, *6*, 2215–2225.

42. Ferguson, T. R.; Bazant, M. Z. Non-equilibrium thermodynamics of porous electrodes. **2012**, submitted, arXiv:1204.2934v1 [physics.chem-ph].

43. Stanton, L. G.; Bazant, M. Z. Phase separation with anisotropic coherency strain. *submitted, arXiv:1202.1626v1 [cond-mat.mtrl-sci]* **2011**,

44. Sekimoto, K. *Stochastic Energetics*; Springer, 2010.

45. Kampen, N. G. V. *Stochastic Processes in Physics and Chemistry*; North-Holland, 2007; Third edition.

46. Aricò, A. S.; Bruce, P.; Scrosati, B.; Tarascon, J.-M.; van Schalkwijk, W. Nanostructured materials for advanced energy conversion and storage devices. *Nature Materials* **2005**, *4*, 366–377.

47. Whittingham, M. S. Lithium Batteries and Cathode Materials. *Chem. Rev.* **2004**, *104*, 4271–4301.

48. Dunn, B.; Kamath, H.; Tarascon, J.-M. Electrical Energy Storage for the Grid: A Battery of Choices. *Science* **2011**, *334*, 928–935.

49. Huggins, R. A. *Advanced Batteries: Materials Science Aspects*; Springer, 2009.

50. Padhi, A.; Nanjundaswamy, K.; Goodenough, J. Phospho-olivines as Positive-Electrode Materials for Rechargeable Lithium Batteries. *Journal of the Electrochemical Society* **1997**, *144*, 1188–1194.

51. Tarascon, J.; Armand, M. Issues and challenges facing rechargeable lithium batteries. *Nature* **2001**, *414*, 359–367.

52. Tang, M.; Carter, W. C.; Chiang, Y.-M. Electrochemically Driven Phase Transitions in Insertion Electrodes for Lithium-Ion Batteries: Examples in Lithium Metal Phosphate Olivines. *Annual Review of Materials Research* **2010**, *40*, 501–529.

53. Kang, B.; Ceder, G. Battery materials for ultrafast charging and discharging. *Nature* **2009**, *458*, 190–193.

54. Meethong, N.; Huang, H.-Y. S.; Carter, W. C.; Chiang, Y.-M. Size-Dependent Lithium Miscibility Gap in Nanoscale $Li_{1-x}FePO_4$. *Electrochem. Solid-State Lett.* **2007**, *10*, A134–A138.

55. Malik, R.; Zhou, F.; Ceder, G. Kinetics of non-equilibrium lithium incorporation in $LiFePO_4$. *Nature Materials* **2011**, *10*, 587–590.

56. Wagemaker, M.; Singh, D. P.; Borghols, W. J.; Lafont, U.; Haverkate, L.; Peterson, V. K.; Mulder, F. M. Dynamic Solubility Limits in Nanosized Olivine LiFePO4. *J. Am. Chem. Soc.* **2011**, *133*, 10222Ð10228.

57. Morgan, D.; der Ven, A. V.; Ceder, G. Li Conductivity in Li_xMPO_4 (M=Mn,Fe,Co,Ni) Olivine Materials. *Electrochemical and Solid State Letters* **2004**, *7*, A30–A32.

58. Malik, R.; Burch, D.; Bazant, M.; Ceder, G. Particle size dependence of the ionic diffusivity. *Nano Letters* **2010**, *10*, 4123–4127.

59. Meethong, N.; Huang, H. Y. S.; Speakman, S. A.; Carter, W. C.; Chiang, Y. M. Strain Accommodation during Phase Transformations in Olivine-Based Cathodes as a Materials Selection Criterion for High-Power Rechargeable Batteries. *Adv. Funct. Mater.* **2007**, *17*, 1115Ð1123.

60. der Ven, A. V.; Garikipati, K.; Kim, S.; Wagemaker, M. The Role of Coherency Strains on Phase Stability in Li_xFePO_4: Needle Crystallites Minimize Coherency Strain and Overpotential. *J. Electrochem. Soc.* **2009**, *156*, A949ÐA957.

61. der Ven, A. V.; Wagemaker, M. Effect of surface energies and nano-particle size distribution on open circuit voltage of Li-electrodes. *Electrochemistry Communications* **2009**, *11*, 881Ð884.

62. Wagemaker, M.; Mulder, F. M.; der Ven, A. V. The Role of Surface and Interface Energy on Phase Stability of Nanosized Insertion Compounds. *Advanced Materials* **2009**, *21*, 2703Ð2709.

63. Oyama, G.; Yamada, Y.; ichi Natsui, R.; ichi Nishimura, S.; Yamada, A. Kinetics of Nucleation and Growth in Two-Phase Electrochemical Reaction of LixFePO4. *J. Phys. Chem. C* **2012**,

64. Dreyer, W.; Jamnik, J.; Guhlke, C.; Huth, R.; Moskon, J.; Gaberscek, M. The thermodynamic origin of hysteresis in insertion batteries. *Nat. Mater.* **2010**, *9*, 448–453.

65. Dreyer, D.; Guhlke, C.; Huth, R. The behavior of a many-particle electrode in a lithium-ion battery. *Physica D* **2011**, *240*, 1008–1019.

66. Burch, D. *Intercalation Dynamics in Lithium-Ion Batteries*; Ph.D. Thesis in Mathematics, Massachusetts Institute of Technology, 2009.

67. Chen, G.; Song, X.; Richardson, T. Electron Microscopy Study of the $LiFePO_4$ to $FePO_4$ Phase Transition. *Electrochemical and Solid State Letters* **2006**, *9*, A295–A298.

68. Bazant, M. Z.; Squires, T. M. Induced-charge electrokinetic phenomena. *Current Opinion in Colloid and Interface Science* **2010**, *15*, 203–213.

69. Bazant, M. Z.; Squires, T. M. Induced-charge electro-kinetic phenomena: Theory and microfluidic applications. *Phys. Rev. Lett.* **2004**, *92*, 066101.

70. Squires, T. M.; Bazant, M. Z. Induced-charge electro-osmosis. *J. Fluid Mech.* **2004**, *509*, 217–252.

71. Bazant, M. Z. *Mathematical Modeling of Electrochemical Energy Systems*; Massachusetts Institute of Technology, 2009; lecture notes for subject 10.95.

72. Bai, P.; Cogswell, D. A.; Bazant, M. Z. International Meeting on Lithium-Ion Batteries, Montreal, Canada, July, 2010.

73. Bazant, M. Z. Meeting of the Electrochemical Society, Las Vegas, NV, October, 2010.

74. Brownian Motion and Nonequilibrium Statistical Mechanics. *Science* **1986**, *233*, 330–334.

75. Vineyard, G. H. Frequency factors and isotope effects in solid state rate processes. *J. Phys. Chem. Solids* **1957**, *3*, 121–127.

76. Kaxiras, E. *Atomic and Electronic Structure of Solids*; Cambridge University Press, 2003.

77. Kramers, H. A. Brownian motion in a field of force and the diffusion model of chemical reactions. *Physica* **1940**, *7*, 284Ð304.

78. Zusman, L. D. Outer-sphere electron transfer in polar solvents. *Chem. Phys.* **1980**, *49*, 295–304.

79. Nauman, E. B.; Heb, D. Q. Nonlinear diffusion and phase separation. *Chemical Engineering Science* **2001**, *56*, 1999Ð2018.

80. Rosso, M. Electrodeposition from a binary electrolyte: new developments and applications. *Electrochimica Acta* **2007**, *53*, 250Ð256.

81. Assadi, H. Phase-field modelling of electro-deoxidation in molten salt. *Modelling and Simulation in Materials Science and Engineering* **2006**, *14*, 963Ð974.

82. Shibuta, Y.; Okajima, Y.; Suzuki, T. A phase-field simulation of bridge formation process in a nanometer-scale switch. *Scripta Materialia* **2006**, *55*, 1095Ð1098.

83. Pongsaksawad, W.; Powell, A. C.; Dussault, D. Phase-Field modeling of Transport-Limited electrolysis in solid and liquid states. *Journal of The Electrochemical Society* **2007**, F122ÐF133.

84. Karma, A. Phase-field model of eutectic growth. *Physical Review E* **1994**, *49*, 2245Ð2250.

85. Boettinger, W.; Warren, J. The phase-field method: Simulation of alloy dendritic solidification during recalescence. *Metallurgical and Materials Transactions A* **1996**, *27*, 657Ð669.

86. Boettinger, W.; Coriell, S.; Greer, A.; Karma, A.; Kurz, W.; Rappaz, M.; Trivedi, R. Solidification microstructures: Recent developments, future directions. *Acta Materialia* **2000**, *48*, 43Ð70.

87. Boettinger, W.; Warren, J.; Beckermann, C.; Karma, A. Phase-field simulation of solidification. *Annual Review of Materials Research* **2002**, *32*, 163Ð194.

88. Bazant, M. Z.; Chu, K. T.; Bayly, B. J. Current-voltage relations for electrochemical thin films. *SIAM J. Appl. Math.* **2005**, *65*, 1463–1484.

89. Biesheuvel, P. M.; van Soestbergen, M.; Bazant, M. Z. Imposed currents in galvanic cells. *Electrochimica Acta* **2009**, *54*, 4857–4871.

90. Cahn, J. W.; Hilliard, J. W. Free energy of a non-uniform system: I. Interfacial energy. *J. Chem Phys.* **1958**, *28*, 258–267.

91. Sequeira, C.; Hooper, A. The study of lithium electrode reversibility against $(PEO)_xLiF_3CSO_3$ polymeric electrolytes. *Solid State Ionics* **1983**, *9Ð10*, 1131Ð1138.

92. Bourderau, S.; Brousse, T.; Schleich, D. Amorphous silicon as a possible anode material for Li-ion batteries. *Journal of Power Sources* **1999**, *81Ð82*, 233Ð236.

93. Park, M.-H.; Kim, M. G.; Joo, J.; Kim, K.; Kim, J.; Ahn, S.; Cui, Y.; Cho, J. Silicon Nanotube Battery Anodes. *Nano Lett.* **2009**, *9*, 3844Ð3847.

94. Mohapatra, S. K. Electrochromism in Li_xWO_3. *J. Electrochem. Soc.* **1975**, *125*, 284–288.

95. Crandall, R. S.; Faughnan, B. W. Dynamics of coloration of amorphous electrochromic films of W03 at low voltages. *Applied Physics Letters* **1976**, *28*, 95–97.

96. Raistrick, I. D.; Mark, A. J.; Huggins, R. A. Thermodynamics and kinetics of the electrochemical insertion of lithium into tungsten bronzes. *Solid State Ionics* **1981**, *5*, 351–354.

97. OÕHayre, R.; Cha, S.; Colella, W.; Prinz, F. B. *Fuel Cell Fundamentals*, second edition ed.; Wiley, 2009.

98. Chueh, W. C.; Lai, W.; Haile, S. M. *Solid State Ionics* **2008**, *179*, 1036Ð1041.

99. Goodwin, D. G.; Zhu, H.; Colclasure, A. M.; Kee, R. J. Modeling Electrochemical Oxidation of Hydrogen on NiÐYSZ Pattern Anodes. *J. Electrochem. Soc.* **2009**, *156*, B1004–B1021.

100. Ciucci, F.; Chueh, W. C.; Goodwin, D. G.; Haile, S. M. Surface reaction and transport in mixed conductors with electrochemically-active surfaces: a 2-D numerical study of ceria. *Phys. Chem. Chem. Phys.* **2011**, *13*, 2121Ð2135.

101. Ioselevich, A. S.; Kornyshev, A. A. Phenomenological Theory of Solid Oxide Fuel Cell Anode. *Fuel Cells 1*, 40–65.

102. Bradwell, D. J.; Kim, H.; Sirk, A. H. C.; Sadoway, D. R. Magnesium?Antimony Liquid Metal Battery for Stationary Energy Storage. *J. Am. Chem. Soc.* **2012**, *134*, 1895?1897.

103. Grjotheim, K.; Krohn, C.; Malinovsky, M.; Matiasovsky, K.; Thonstad, J. *Aluminum Electrolysis. The Chemistry of the Hall-Heroult Process*; Aluminium- Verlag GmbH, Dusseldorf, Germany, 1977; Vol. 350.

104. Welton, T. Room-Temperature Ionic Liquids. Solvents for Synthesis and Catalysis. *Chem.Rev.* **1999**, *99*, 2071–2084.

105. Conway, B. E. *Electrochemical supercapacitors: scientific fundamentals and technological applications*; Springer, 1999.

106. Simon, P.; Gogotsi, Y. Materials for electrochemical capacitors. *Nature Materials* **2008**, *7*, 845–854.

107. Kornyshev, A. A. Double-layer in ionic liquids: Paradigm change? *J. Phys. Chem. B* **2007**, *111*, 5545–5557.

108. Lue, L.; Zoeller, N.; Blankschtein, D. Incorporation of Nonelectrostatic Interactions in the Poisson Boltzmann Equation. *Langmuir* **1999**, *15*, 3726–3730.

109. di Caprio, D.; Borkowska, Z.; Stafiej, J. Simple extension of the Gouy-Chapman theory including hard sphere effects: Diffuse layer contribution to the differential capacitance curves for teh electrodelelectrolyte interface. *J. Electroanal. Chem.* **2003**, *540*, 17–23.

110. Levin, Y. Electrostatic correlations: from plasma to biology. *Rep. Prog. Phys.* **2002**, *65*, 1577–1632.

111. Carnahan, N. F.; Starling, K. E. Equation of State for Nonattracting Rigid Spheres. *J. Chem. Phys.* **1969**, *51*, 635–636.

112. Boublik, T. Hard sphere equation of state. *J. Chem. Phys.* **1970**, *53*, 471–472.

113. Mansoori, G. A.; Carnahan, N. F.; Starling, K. E.; Leland, T. W. Equilibrium Thermodynamic Properties of the Mixture of Hard Spheres. *J. Chem. Phys.* **1971**, *54*, 1523–1525.

114. van der Waals, J. D. The thermodynamic theory of capillarity under the hypothesis of a continuous variation of density. *Verhandel. Konink. Akad. Weten. Amsterdam (Sect. 1)* **1893**, *1*, 8, (Translation by J. S. Rowlinson, J. Stat. Phys. 1979, 20, 197-244).

115. Cahn, J. Free Energy of a Nonuniform System. II. Thermodynamic basis. *Journal of Chemical Physics* **1959**, *30*, 1121–1124.

116. Cahn, J.; Hilliard, J. Free Energy of a Nonuniform System. III. Nucleation in a two-component incompressible fluid. *Journal of Chemical Physics* **1959**, *31*, 688–699.

117. Cahn, J. On spinodal decomposition. *Acta Metallurgica* **1961**, *9*, 795–801.

118. Landau, L.; Lifshitz, E. *Statistical Physics*; Butterworth-Heinemann, 1980.

119. de Gennes, P. G. *Superconductivity of Metals and Alloys*; Perseus Books, 2nd Ed., 1995.

120. Gupta, K. M. PhD thesis, Department of Materials Science and Engineering, Massachusetts Institute of Technology.

121. Chen, L. Q.; Khachaturyan, A. G. Dynamics of simultaneous ordering and phase separation and effect of long-range coulomb interactions. *Phys. Rev. Lett.* **1993**, *70*, 1477Ð80.

122. Bishop, C. M.; Garcia, R. E.; Carter, W. C. Effect of charge separation on the stability of large wavelength fluctuations during spinodal decomposition. *Acta Materialia* **2003**, *51*, 1517–1524.

123. Allen, S.; Cahn, J. Microscopic theory for antiphase boundary motion and its application to antiphase domain coarsening. *Acta Metallurgica* **1979**, *27*, 1085Ð1095.

124. Laffont, L.; Delacourt, C.; Gibot, P.; Wu, M. Y.; Kooyman, P.; Masquelier, C.; Tarascon, J. M. Study of the LiFePO4/FePO4 Two-Phase System by High-Resolution Electron Energy Loss Spectroscopy. *Chem. Mater.* **2006**, *18*, 5520–5529.

125. Burch, D. N.; Bazant, M. Z. Design principle for improved three-dimensional ac electro-osmotic pumps. *Phys. Rev. E* **2008**, *77*, 055303(R).

126. Aziz, M. J.; Sabin, P. C.; Lu, G. Q. The activation strain tensor: Nonhydrostatic stress effects on crystal growth kinetics. *Phys. Rev. B 41*, 9812–9816.

127. Frumkin, A. Wasserstoffüberspannung und Struktur der Doppelschict. *Z. Phys. Chem.* **1933**, *164A*, 121–133.

128. Itskovich, E. M.; Kornyshev, A. A.; Vorotyntsev, M. A. Electric Current across the Metal-Solid Electrolyte Interface. I. Direct Current, Current-Voltage Characteristic. *phys. stat. sol. (a)* **1977**, *39*, 229–238.

129. Kornyshev, A. A.; Schmickler, W.; Vorotyntsev, M. A. Nonlocal electrostatic approach to the problem of a double layer at a metal-electrolyte interface. *Phys. Rev. B* **1982**, *25*, 5244–5256.

130. Biesheuvel, M.; Franco, A. A.; Bazant, M. Z. Diffuse-charge effects in fuel-cell membranes. *Journal of the Electrochemical Society* **2009**, *156*, B225–B233.

131. Bonnefont, A.; Argoul, F.; Bazant, M. Analysis of diffuse-layer effects on time-dependent interfacial kinetics. *J. Electroanal. Chem.* **2001**, *500*, 52–61.

132. Chu, K. T.; Bazant, M. Z. Electrochemical thin films at and above the classical limiting current. *SIAM J. Appl. Math.* **2005**, *65*, 1485–1505.

133. Biesheuvel, P.; Bazant, M. Nonlinear dynamics of capacitive charging and desalination by porous electrodes. *Physical Review E* **2010**, *81*.

134. Biesheuvel, P.; Fu, Y.; Bazant, M. Diffuse charge and Faradaic reactions in porous electrodes. *Physical Review E* **2011**, *83*.

135. Biesheuvel, P.; Fu, Y.; Bazant, M. Electrochemistry and capacitive charging of porous electrodes in asymmetric multicomponent electrolytes. *Russian Journal of Electrochemistry* **2012**,

136. Nauman, E. B.; Balsara, N. P. Phase Equilibria and the Landau-Ginzburg Functional. *Fluid Phase Equilib.* **1989**, *45*, 229Ð250.

137. Islam, M. S.; Driscoll, D. J.; Fisher, C. A. J.; Slater, P. R. Atomic-scale investigation of defects, dopants, and lithium transport in the LiFePO4 olivine-type battery material. *Chem. Mater.* **2005**, *17*, 5085Ð5092.

138. Doyle, M.; Gozdz, A. S.; Schmuts, C. N.; Tarascon, J.-M.; Newman, J. Comparison of modeling predictions with experimental data from plastic lithium ion cells. *Journal of the Electrochemical Society* **1996**, *143*.

139. Delmas, C.; Maccario, M.; Croguennec, L.; Cras, F. L.; Weill, F. Lithium deintercalation of $LiFePO_4$ nanoparticles via a domino-cascade model. *Nature Materials* **2008**, *7*, 665–671.

140. Tang, M.; Belak, J. F.; Dorr, M. R. Anisotropic phase boundary morphology in nanoscale olivine electrode particles. *The Journal of Physical Chemistry C* **2011**, *115*, 4922–4926.

141. Zhu, Y.; Wang, C. Galvanostatic intermittent titration technique for phase-transformation electrodes. *Journal of Physical Chemistry C* **2010**, *114*, 2830–2841.

142. Ramana, C. V.; Mauger, A.; Gendron, F.; Julien, C. M.; Zaghib, K. Study of the Li-Insertion/Extraction Process in $LiFePO_4$/ $FePO_4$. *J. Power Sources* **2009**, *187*, 555Ð564.

143. Cahn, J. W. Critical point wetting. *J. Chem. Phys.* **1977**, *66*, 3667–3672.

144. Sun, K.; Dillon, S. J. A mechanism for the improved rate capability of cathodes by lithium phosphate surficial films. *Electrochemistry Communications* **2011**, *13*, 200–202.

145. Newman, J.; Thomas-Alyea, K. *Electrochemical Systems*, 3rd ed.; Wiley-Interscience, 2004.

146. Harris, S. J.; Timmons, A.; Baker, D. R.; Monroe, C. Direct in situ measurements of Li transport in Li-ion battery negative electrodes. *Chemical Physics Letters* **2010**, *485*, 265Ð274.

147. Ramadesigan, V.; Northrop, P. W. C.; De, S.; Santhanagopalan, S.; Braatz, R. D.; Subramanian, V. R. Modeling and Simulation of Lithium-Ion Batteries from a Systems Engineering Perspective. *Journal of The Electrochemical Society* **2012**, *159*, R31–R45.